THE ASTROPHYSICAL JOURNAL, 382:416–432, 1991 December 1

OUTFLOWS DRIVEN BY COSMIC-RAY PRESSURE IN BROAD ABSORPTION LINE QSOs

MITCHELL C. BEGELMAN[1,2] AND MARTIJN DE KOOL[3]
Joint Institute for Laboratory Astrophysics, University of Colorado and National Institute of Standards and Technology, Boulder, CO 80309-0440

AND

MAREK SIKORA
N. Copernicus Astronomical Center, Polish Academy of Sciences, 00-716 Warsaw, Poland
Received 1990 December 20; accepted 1991 May 31

ABSTRACT

We present a model that can explain many features of the very fast ($\sim 0.1c$) outflows that are observed in broad absorption line QSOs (BALQSOs). In our model the wind is accelerated primarily by the pressure of ultrarelativistic protons. These protons are deposited in the wind, over a range of radii, by the decay of ultrarelativistic neutrons escaping from the central engine. Recent models for nonthermal processes in the central engines of active galactic nuclei (AGNs) predict a neutron luminosity which can exceed a few percent of the radiation flux, which is more than adequate to accelerate the wind. Since the energy deposition is predicted to peak at distances of order 1–10 pc, the main acceleration will occur outside the broad emission line region, as seems to be required by observations.

The absorbing gas occupies a very small fraction of the volume of the wind, and must be confined by it. Keeping this gas sufficiently cool in the radiation field from the central source requires that the pressure in the absorbing clouds or filaments be higher than a certain value. Since the relativistic protons can pass right through the clouds, the confinement of the clouds is most likely to be due to thermal pressure in the wind. This is possible only if the energy of the ultrarelativistic protons can be converted to thermal energy with a high efficiency. We suggest that this might be accomplished through the excitation and subsequent damping of Alfvén waves, or by a turbulent wind structure containing shocks that will drive the thermal and cosmic-ray energy densities to equipartition. We discuss and evaluate the plausibility of other confinement mechanisms as well.

A simple model in which the absorption is caused by a fine spray of cloudlets, comoving with the wind and in pressure equilibrium with it, can reproduce a wide variety of BAL profiles similar to those that are observed. Line profiles prove to be more sensitive to ionization effects than to the details of the wind dynamics, thus making it difficult to derive the dynamical properties of the wind from the line profiles. We find that a self-consistent treatment of internal absorption in the wind can play an important role, both in reproducing the observed ionization levels and in explaining certain line features.

Finally we discuss the formation, acceleration, and survival of the absorbing cloudlets. We argue that the absorbing gas is probably entrained into the wind near its base, and must survive the acceleration. The clouds are forced to comove with the wind by a combination of hydrodynamic drag and line radiation pressure, and are susceptible to dynamical instabilities, as well as thermal evaporation in the hot ambient medium. We point out difficulties with models in which clouds are continuously destroyed and re-form through thermal instability, and suggest several effects which may allow clouds to survive the various destructive influences. The small solid angle apparently subtended by absorbing gas in a BALQSO could reflect a nonspherical distribution of sources for the entrained matter (e.g., a disk or a flattened distribution of large clouds).

Subject headings: cosmic rays: general — hydrodynamics — line profiles — particle acceleration — quasars

1. INTRODUCTION

Between 3% and 10% of QSOs exhibit strong, broad absorption components in ultraviolet resonance lines like those of C IV, Si IV, and N V, which are blueshifted relative to the center of the broad emission line with velocities ranging up to 0.2c (Turnshek 1988). As in stellar P Cygni profiles, this absorption has to occur in material which is flowing out from the central source in the direction of the observer. The properties of these so-called broad absorption line QSOs (BALQSOs) have been more recently reviewed by Turnshek (1988, hereafter T88) and Weymann, Turnshek, & Christiansen (1985, hereafter WTC), and much of our Introduction follows these papers. The fact that BALs are observed in a small fraction of QSOs can be understood in two different ways. The first possibility is that we are dealing with an aspect effect: most QSOs are BALQSOs, but they are recognized as such only when viewed from special directions. The other possibility is that BALQSOs form a small special population that exhibits BALs in every direction. The first possibility now seems to be generally preferred, because of the absence of any redshifted emission at the velocities seen in the absorption components. A spherical distribution of outflowing material has to produce such emission, and its absence can be used to constrain the solid angle over which the absorbing outflow occurs to less than 1 sr. Since this

[1] Alfred P. Sloan Foundation Research Fellow.

[2] Also at Department of Astrophysical, Planetary, and Atmospheric Sciences, University of Colorado, Boulder.

[3] Postal address: Max-Planck-Institut für Astrophysik, Karl-Schwarzschild-Strasse 1, D-8046 Garching bei München, Germany.

means that a BALQSO can only be recognized as such in 1 out of 10 cases, the observed fraction of BALQSOs implies that a large fraction of QSOs have the kind of outflow observed in BALQSOs, and their study may lead to important clues about the structure of QSOs in general. The interpretation of the BAL phenomenon in terms of viewing angle means that other differences between normal QSOs and BALQSOs (such as a high incidence of optical variability, a relatively high degree of polarization, and unusual weakness of compact radio emission) also have to be explained as aspect effects.

Some constraints on the absorbing material can be derived from the properties of the absorption lines in a very general, model-independent way. There are two strong arguments that the material has to lie outside the broad emission line (BEL) region. The first is that in many systems the Lyα emission line seems to be strongly absorbed by the N V BAL (T88), and the second is that in some systems the blue wing of the BEL is completely absorbed (Turnshek et al. 1988). This last observation implies that there is absorbing material with velocities ranging from very low values ($v < 10^3$ km s^{-1}) to at least the width of the emission line, located outside the BEL region.

A second constraint is on the ionization parameter of the absorbing gas. We have used Ferland's (1989) ionization and thermal equilibrium code CLOUDY to calculate the equilibrium temperatures of optically thin clouds exposed to two different power-law continua, $F_\nu \propto \nu^{-0.7}$ and $F_\nu \propto \nu^{-1.0}$. Since there are indications that the internal column densities of BALQSOs can be quite high (e.g., Singh, Westergaard, & Schnopper 1987), the effect of such an internal column was also investigated. If the equilibrium temperature is expressed as a function of the ionization parameter (the ratio of the radiation pressure of the radiation from the central source to the gas pressure in the cloud), we find the familiar result (e.g., Krolik, McKee, & Tarter 1981) that there is a maximum ionization parameter, $\Xi_{\rm cool}$, above which the cool ($T < 10^5$ K) material that has to be responsible for the BALs cannot exist. $\Xi_{\rm cool}$ ranges from 10 to ~ 30, depending on the amount of absorption.

Requiring the ionization parameter in the cold phase to be less than $\Xi_{\rm cool}$ allows us to place a lower limit on the density in the cold clouds:

$$n_c > 3 \times 10^6 L_{46}\, T_{4.5}^{-1} R_{19}^{-2} \ {\rm cm}^{-3} \,, \tag{1.1}$$

in which $L_{46} \equiv L_\gamma/10^{46}$ ergs s^{-1} is the photon luminosity of the central source, $T_{4.5}$ is the cold-phase temperature in units of $10^{4.5}$ K, and R_{19} is the distance from the nucleus in units of 10^{19} cm. Comparing the velocity widths observed in many BALs with the line width expected for a single cloud leads to the requirement that the number of clouds in the line of sight through the BAL region, $\mathcal{N}_{\rm cl}$, exceed 10^3 (WTC). Simple algebra then leads to the following constraints on the hydrogen column density $N_{\rm H,cl}$, cloud size $R_{\rm cl}$, and volume filling factor $f_{\rm fill}$:

$$N_{\rm H,cl} = \frac{\dot M_{\rm cl}}{4\pi m_p \mathcal{N}_{\rm cl} v R} < 5 \times 10^{16} \dot M_{c,25}\, R_{19}^{-1} v_9^{-1} \ {\rm cm}^{-2} \,, \tag{1.2}$$

$$R_{\rm cl} = \frac{N_{\rm H,cl}}{n_c} < 1.7 \times 10^{10} \dot M_{c,25}\, L_{46}^{-1} T_{4.5} R_{19} v_9^{-1} \ {\rm cm} \,, \tag{1.3}$$

$$f_{\rm fill} = \mathcal{N}_{\rm cl} \frac{R_{\rm cl}}{R} < 1.6 \times 10^{-6} \dot M_{c,25}\, L_{46}^{-1} T_{4.5} v_9^{-1} \,, \tag{1.4}$$

in which $\dot M_{c,25}$ is the mass-loss rate in clouds in units of 10^{25} g s^{-1} (per 4π sr) and v_9 is the velocity in units of 10^9 cm s^{-1}. Even though these estimates are very crude and could easily be off by an order of magnitude, the conclusion that the absorbing clouds are extremely small (like a fine mist or spray) seems to be inescapable. Note that more than 10^6 clouds are necessary just to cover the central engine.

The fact that there is absorbing material with a wide range of velocities from 0 to $\sim 0.1c$ outside the BEL region (i.e., at $R \gtrsim 1$ pc) is quite remarkable, since most conventional acceleration mechanisms for outflows in AGNs, such as radiation pressure, are expected to operate at a much smaller radius, and the wind would be close to its terminal velocity by the time it has crossed the BEL region. This difficulty can possibly be overcome by assuming that the velocity of the outflow is actually decreasing outward—for instance, as the result of the "loading" of an initially fast outflow with extra mass due to entrainment. However, no plausible deceleration model has yet been constructed, and we will concentrate on models employing accelerating outflows.

In a number of recent papers (Sikora, Begelman, & Rudak 1989; Kirk & Mastichiadis 1989; Begelman, Rudak, & Sikora 1990, hereafter BRS) on the consequences of high-energy processes occurring in the central engine of an AGN, it has been shown that a significant part of the luminosity generated in such objects could escape in the form of a flux of ultrarelativistic neutrons. These neutrons are created by inelastic proton-proton collisions and photomeson reactions involving protons accelerated up to energies as large as 10^7–10^8 GeV. Because of relativistic time dilation, neutrons with Lorentz factor γ can travel a distance $\sim 10^{-5}\gamma$ pc before decaying. The relativistic protons resulting from neutron decay are trapped by the local magnetic field, and their energy may be used for bulk acceleration and heating of the ambient gas. BRS estimate that most of the neutron energy will be deposited between 1 and 10 pc (see also § 2), and they point out that this energy deposition could easily drive an outflow with the main acceleration occurring in the radius range required for BALQSOs. In this paper we investigate this idea (which in its dynamical aspects bears some similarity to the model by Weymann et al. 1982 for the BEL region) in more detail. In § 2 we review the theory of neutron production and escape, and determine the dynamical and thermal structure of a wind driven by the protons created by neutron decay. In § 3 we model the formation of BALs in such an outflow, deriving line profiles and constraining the rate at which the energy of relativistic protons has to be converted to thermal energy in order to provide pressure confinement for the BAL clouds. In § 4 we discuss the problem of acceleration and survival of the clouds, and consider some alternative confinement mechanisms. We summarize our results in § V and discuss some general points, such as the likely geometry of the outflow.

2. THEORY OF NEUTRON-DRIVEN WINDS

2.1. *Cosmic-Ray Energy Deposition and Losses*

The energy distribution of the relativistic neutrons escaping from the central engine is discussed in detail by BRS. The neutrons are produced as a result of collisions of very energetic protons (γ_p up to 10^7–10^8), accelerated in shocks in the central engine, with ambient photons and thermal protons. Proton-photon ($p\gamma$) collisions are the dominant production mechanism for high-energy neutrons, whereas proton–proton (pp) collisions are responsible for the lower energy neutrons. The emerging neutron spectrum can be divided into four regimes, according to the relative importance of the physical processes shaping the spectrum. These processes (and the associated inverse time scales, which are a measure of their importance) are (1) neutron escape ($t_{\rm esc}^{-1}$); (2) $p\gamma$ and $n\gamma$ collisions (photomeson reactions), which are responsible for the production and the destruction of neutrons (t_γ^{-1}); (3) inelastic pp and np collisions, which also produce and destroy neutrons (t_{pp}^{-1}, t_{np}^{-1}); and (4) advection, through which protons are removed from the central engine by either accretion onto the black hole or ejection in a wind ($t_{\rm ad}^{-1}$).

The relative importance of these processes varies with both particle energy and local physical conditions. For simple estimates of the conditions expected in the central engine of an AGN (summarized in Fig. 1 of BRS and the accompanying text), BRS found the following regimes (Fig. 1). In the lowest energy regime (I), $t_{\rm ad}^{-1} > (t_\gamma^{-1} + t_{pp}^{-1})$ and $t_{pp}^{-1} > t_\gamma^{-1}$. This means that the proton spectrum in the source has the same slope as the proton injection spectrum, and neutron production occurs mainly by pp collisions. The neutrons escape freely (as they do also in regimes II and III), and their spectrum parallels that of the protons. In regime II we still have $t_{\rm ad}^{-1} > (t_\gamma^{-1} + t_{pp}^{-1})$, but now $t_\gamma^{-1} > t_{pp}^{-1}$. The proton spectrum in the source is the same as in regime I, but the neutrons are produced primarily by $p\gamma$ collisions. Regime II is separated from regime I by the energy γ_{pp} at which $t_\gamma = t_{pp}$. Most neutron-producing reactions occur close to the energy threshold, and because the photon number density increases with decreasing photon energy, the neutron spectrum is flatter (or decreases less steeply with energy) than that of the protons. In regimes I and II most protons are lost by advection before they interact, hence only a small fraction of the injected energy is converted

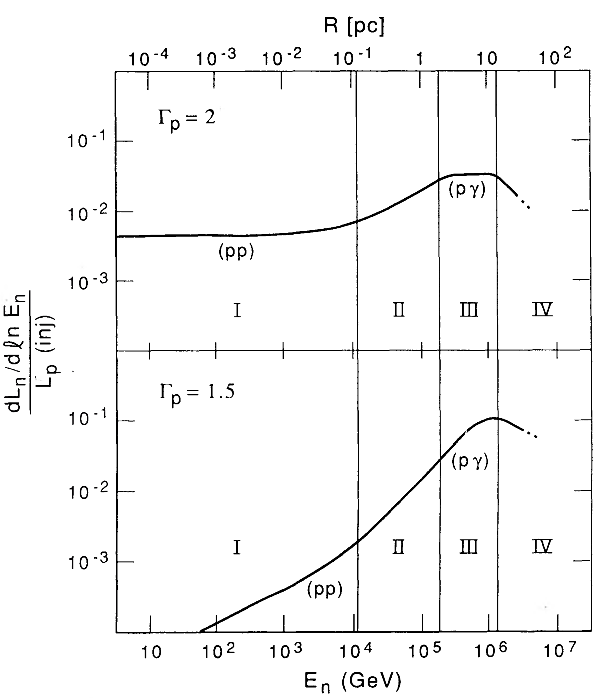

FIG. 1.—Spectra of the relativistic neutron flux from the central engine of an AGN, after Begelman, Rudak, & Sikora (1990). The spectra shown are for assumed proton injection spectra $Q_p \propto \gamma_p^{-2}$ and $Q_p \propto \gamma_p^{-1.5}$. The roman numerals I, II, III and IV refer to the different physical regimes described in the text.

into reaction products like neutrons. In regime III we have $t_{\rm ad}^{-1} < t_\gamma^{-1}$ and $t_{pp}^{-1} \ll t_\gamma^{-1}$. At these energies the proton spectrum in the source no longer has the same slope as the proton injection spectrum, but is determined by the equilibrium between injection and losses due to $p\gamma$ collisions, which are also responsible for the production of neutrons. In this regime the conversion of relativistic proton energy into escaping neutron flux is most efficient. Finally, in regime IV the processes producing neutrons are the same as in III, but now t_γ^{-1}, which is also a measure of the importance of neutron absorption, becomes larger than $t_{\rm esc}^{-1}$. This means that the neutrons can no longer escape freely from the central engine, which causes a break in the spectrum and a steepening toward higher energies. In Figure 1 (adapted from Fig. 7 of BRS) the escaping neutron spectrum is given for a primary proton injection function (by number) which is a power law in energy, $Q_p \propto \gamma_p^{-\Gamma_p}$. In this case the shape of the neutron spectrum in the different regimes is also a power law:

$$\frac{dL_n}{d\ln\gamma_n} \propto \gamma_n^{-\Gamma_n} , \tag{2.1}$$

with $\Gamma_{n,\rm I} = \Gamma_p - 2$, $\Gamma_{n,\rm II} = \Gamma_p - 3$, $\Gamma_{n,\rm III} = \Gamma_p - 2$ and $\Gamma_{n,\rm IV} = \Gamma_p - 1$. The spectrum in regime IV depends on transfer effects, and thus may vary with the geometry of the source. The positions of the breaks in this spectrum that signify the transitions between the regimes do depend on the specific parameters of the central engine, and the reader is referred to BRS and to Sikora et al. (1989) for a discussion of the model used to construct Figure 1. In particular, the characteristic energies at the breaks scale roughly inversely with the "radiation compactness" of the source, $\ell = (L/R)(\sigma_{\rm T}/4\pi m_e c^3) \sim 100L/L_{\rm Edd}$, where $\sigma_{\rm T}$ is the Thomson cross section and $L_{\rm Edd}$ is the Eddington limit. For QSO–like sources with a sufficiently flat proton injection function ($\Gamma_p \leq 2$) and ℓ in the range 1–10, the bulk of the neutron luminosity will be emitted around $\gamma_n \approx 10^5$–10^6. Because of relativistic time dilation these neutrons will decay at a distance of the order of 1–10 pc from the central engine.

We assume that neutrons escaping from the central engine travel ballistically until they decay, at which point the resulting protons are trapped locally by the magnetic field. We neglect the small amount of energy carried by the electron and the neutrino produced during decay. The energy deposition rate per unit volume in relativistic protons ("cosmic rays") at radius R is therefore given by

$$H_{\rm CR}(R) = \left(\frac{dL_n/d\ln\gamma_n}{4\pi R^3}\right)_{\gamma_n = R/c\tau_n} \equiv \frac{L'_{\rm CR}(R)}{4\pi R^3} , \tag{2.2}$$

where $\tau_n \simeq 10^3$ s is the mean neutron lifetime in its rest frame and the computation of the neutron energy distribution $dL_n/d\ln\gamma_n$ is discussed above. $L'_{\rm CR}(R)$ is therefore the rate of neutron energy deposition per logarithmic range of radius. The assumption that the neutrons travel unimpeded is valid provided that the column density along the trajectory is less than $1/\sigma^{(pp)} \simeq 2.5 \times 10^{25}$ cm^{-2}, where $\sigma^{(pp)}$ is the cross section for inelastic pp collisions with thermal protons. Photomeson reactions can be neglected well outside the neutron production region.

Relativistic protons deposited by neutron decay lose energy through inelastic collisions with background protons, at a rate per unit volume given by

$$C_{\rm CR}^{(pp)} = 3p_{\rm CR}\, n_p c\sigma^{(pp)} K^{(pp)} , \tag{2.3}$$

where p_{CR} is the cosmic-ray pressure, n_p is the density of thermal protons and $K^{(pp)} \simeq \frac{1}{2}$ is the mean inelasticity for pp collisions. The quantity $n_p c\sigma^{(pp)} K^{(pp)}$ is simply the proton cooling rate $(t_p)^{-1}$ which is introduced in BRS. $C_{CR}^{(pp)}$ generally exceeds the corresponding energy loss rate for neutrons because the density of magnetically trapped protons exceeds that of the freely streaming neutrons.

The cosmic rays are subject to other losses as well. Because most of the energy resides in protons with Lorentz factors $\gamma_p \gg 100$, Coulomb losses are negligible compared with losses through pp collisions. However, the cosmic rays will excite Alfvén waves as they try to stream through the background plasma. Since the background medium is expected to be highly ionized, wave damping will be weak and the cosmic ray (CR) particles will be effectively scattered and dynamically coupled to the plasma. Losses through excitation of (damped) Alfvén waves give a volume cooling rate

$$C_{CR}^{(A)} = -\boldsymbol{v}_{CR} \cdot \nabla p_{CR} , \qquad (2.4)$$

where v_{CR} is the streaming speed of cosmic rays relative to the thermal background plasma (Wentzel 1974). If the Alfvén waves are excited by the streaming cosmic rays, then v_{CR} should approximately equal the radial component of the Alfvén speed v_A (Skilling 1975).

Finally, we must consider the spatial diffusion of cosmic rays relative to the scattering centers. The characteristic diffusion speed of cosmic rays parallel to the magnetic field is $v_{diff} \sim D_{\parallel}/l$, where $l \sim R$ is the scale length of the CR pressure gradient,

$$D_{\parallel} \simeq \frac{cR_L}{3}\left(\frac{\delta B}{B}\right)^{-2} \qquad (2.5)$$

is the spatial diffusion coefficient (Blandford & Eichler 1987), and $R_L = \gamma_p m_p c^2/eB$ is the Larmor radius. Since the background plasma is likely to be very highly ionized, the minimal level of Alfvén turbulence is estimated by balancing the wave growth rate [which can be expressed in terms of the wave intensity $(\delta B/B)^2$ and the loss rate $C_{CR}^{(A)}$] against the nonlinear (three-wave) damping rate (Wentzel 1974). We obtain the result (which must be regarded as extremely crude, given the assumptions)

$$\left(\frac{\delta B}{B}\right)^2 \sim \left[\left(\frac{v_A}{v_i + v_A}\right)\left(\frac{p_{CR}}{p_{mag}}\right)\left(\frac{R_L}{R}\right)\right]^{1/2} \qquad (2.6)$$

and

$$\frac{v_{diff}}{c} \sim \frac{1}{3}\left[\left(\frac{v_i + v_A}{v_A}\right)\left(\frac{p_{mag}}{p_{CR}}\right)\left(\frac{R_L}{R}\right)\right]^{1/2} , \qquad (2.7)$$

where $p_{mag} = B^2/8\pi$ and $v_i = (kT/m_p)^{1/2}$ (Loewenstein, Zweibel, & Begelman 1991). In equation (2.7), the product of the first two factors inside the square brackets is of order $(p_{th} + p_{mag})^{1/2} p_{mag}^{1/2}/p_{CR}$ (where p_{th} is the thermal pressure), which is clearly less than 1 in a wind driven by cosmic-ray pressure. Since the CR pressure in a particular region is dominated by the protons injected locally by decaying neutrons, we have $R_L/R \sim 10^{-7}/B$ (where B is in gauss) (Sikora et al. 1989). Thus, provided that B is not much smaller than 10^{-3} G, we estimate that v_{diff} will be of order 10^3 km s^{-1} or less, i.e., small compared with typical flow speeds. If the magnetic field is tangled, the diffusion rate will be smaller. We will therefore neglect large-scale diffusion in our analysis of neutron-driven winds, bearing in mind that it may be important in smoothing out CR pressure gradients over small scales, e.g., between a cloud and the surrounding intercloud medium, and in high-density regions near the base of the wind. We will ultimately argue that most of the CR energy goes into the kinetic energy of the wind, through adiabatic expansion.

2.2. *Thermal Properties of the Wind*

The products of inelastic pp reactions—pairs and γ-rays—do not effectively heat the thermal plasma in the wind. The conversion rate of CR energy to thermal energy due to plasma processes is therefore likely to be dominated by the damping of Alfvén waves generated as a result of CR streaming, and we investigate this process in more detail now. The conversion rate is approximately given by $C_{CR}^{(A)} \sim p_{CR} v_{CR}/R$. Estimating $p_{CR} \sim H_{CR} R/3v$ in the accelerating region of the flow, we obtain $C_{CR}^{(A)} \sim H_{CR}(v_{CR}/3v)$, where v_{CR}, the radial streaming speed of CR relative to the plasma, is expected to be close to the radial component of the Alfvén speed, $B_R/(4\pi\rho)^{1/2}$. Unfortunately, we know neither the strength nor the structure of the magnetic field, so we must leave v_{CR} as a parameter. In addition to $C_{CR}^{(A)}$ the wind is subject to a variety of radiative heating and cooling processes, including atomic line radiation (at $T \lesssim 10^6$ K), Compton heating and cooling, and bremsstrahlung. Following the conventions used in Begelman & McKee (1990), we write the net radiative cooling rate for the gas (assumed to be at $T \gtrsim 10^6$ K) in the form

$$C_{th} \equiv n_h^2 \mathscr{L} = n_h^2(\Lambda_{IC} + \Lambda_{br}) - n_h \Gamma_{IC} , \qquad (2.8)$$

where $\mathscr{L}$ is the net cooling function, Γ_{IC} and Λ_{IC} are the Compton heating cooling functions, respectively, Λ_{br} is the bremsstrahlung cooling function, and n_h is the density in the "hot" phase.

We nondimensionalize the cooling rate by normalizing pressures to the radiation energy density $u_\gamma = L_\gamma/4\pi R^2 c$, temperatures to the inverse Compton temperature $T_{IC} = 10^7 T_{IC7}$ K, and heating/cooling rates to the Compton heating rate $\Gamma_{IC} = 4\sigma_T u_\gamma kT_{IC}/m_e c$. Dimensionless quantities are denoted by an asterisk. In this notation, the thermal pressure p_{th} satisfies $p_{th}^{*-1} = \Xi$, where Ξ is the ionization parameter, and the normalized density is given by $n^* = p_{th}^*/T^*$. The energy equation of the thermal gas may then be expressed in the form

$$\frac{3}{8\ell}\left(\frac{v}{c}\right)\frac{d}{d\ln R}\ln\left(\frac{p_{th}}{n_h^{5/3}}\right) = -1 - \frac{\Xi_{CB} p_{th}^*}{T^{*3/2}} + \frac{1}{T^*} + \frac{1}{4\ell}\left|\frac{d\ln p_{CR}}{d\ln R}\right|\left(\frac{p_{CR}}{p_{th}}\right)\left(\frac{v_{CR}}{c}\right) , \qquad (2.9)$$

where $\ell \equiv L_\gamma \sigma_T/4\pi R m_e c^3 = 2 \times 10^{-3} L_{46} R_{19}^{-1}$ is the "radiation compactness" at R, and $\Xi_{CB} = 14.9 T_{IC7}^{-3/2}$ is a fiducial value of the ionization parameter at which bremsstrahlung cooling at T_{IC} balances Compton heating (Begelman & McKee 1990).

Because ℓ is so small in the wind acceleration zone, radiative heating and cooling processes (the first three terms on the right-hand side of eq. [2.9]) become relatively insignificant compared with adiabatic cooling and cosmic-ray heating when the wind speed exceeds a few thousand kilometers per second. Therefore, for all but the initial acceleration stage the thermal state of the wind is determined by the balance between these nonradiative heating and cooling processes, and the equilibrium thermal pressure adjusts to

$$p_{th} \approx \zeta p_{CR}\left(\frac{v_{CR}}{v}\right) , \qquad (2.10)$$

where ζ depends on the details of the flow. Determining the value of ζ can be important for understanding the thermal behavior of the wind. For example, consider an acceleration zone in which $\dot{M} \sim$ constant and $H_{CR} \propto R^{-3}$. The velocity increases slowly with R and estimating $p_{CR} \sim H_{CR} R/3v$ (in rough agreement with our numerical calculations), we may take $p_{CR} \propto R^{-2}$. If the radial component of the magnetic field varies as R^{-2}, as predicted by the naive scaling from flux freezing, then $v_{CR} \propto R^{-1}$ and $\zeta = 4$. If $v_{CR} \propto v$, as might be the case in the presence of strong dynamo action in the wind (§ 4), then $\zeta = 1$. Demanding that $p_{th} > p_{rad}/\Xi_{cool}$ in order for absorbing clouds to be in thermal equilibrium (§ 1) leads to the condition that

$$\left(\frac{v_{CR}}{v}\right) > 3\zeta^{-1}\left(\frac{L_\gamma}{10L'_{CR}}\right)\left(\frac{\Xi_{cool}}{10}\right)^{-1}\left(\frac{v}{c}\right). \tag{2.11}$$

Thus, if the thermal pressure of the CR–heated wind is responsible for confining the absorbing filaments, then v_{CR} must be a sizable fraction of v, perhaps as large as several tens of percent, depending on L_γ/L'_{CR}. We discuss possible alternative sources of cloud confinement pressure in § 4.

An interesting feature of the energy balance expressed by equation (2.10) is that the equilibrium thermal pressure does not depend explicitly on the density of the hot gas. Thus, the intercloud medium could have an extremely low density and a temperature much greater than T_{IC}, and still confine the absorbing filaments. Given the constraints on the mass flux in the wind, we find that the temperature of the hot phase would have to be higher than 10^8 K in order to confine the filaments (§ 2.3). Moreover, the functional form of the CR heating rate could give rise to a thermal instability which would tend to drive p_{th} toward p_{CR} by increasing the value of v_{CR}. Cosmic-ray heating is isobarically unstable because the heating rate (for fixed ∇p_{CR} and magnetic field geometry) is proportional to the Alfvén speed, which varies with density as $\rho^{-1/2}$. Thus, a slightly underdense region will be heated more rapidly than an overdense region, giving rise to instability. Since the equilibrium value of p_{th} is independent of n_h, this instability will operate as long as p_{th} is much smaller than p_{CR}. By placing a larger and larger fraction of the wind into cold filaments with a small filling factor, the Alfvén speed of the intercloud medium (and therefore the equilibrium thermal pressure) can increase. We have analyzed this instability using the Lagrangian techniques described by Balbus & Soker (1989), which are applicable to a flowing medium, and can supply the details to interested readers. In agreement with Loewenstein (1990) and Balbus (1991), we find that the dynamical effects of even a small magnetic field are sufficient to cancel the stabilizing effects of buoyancy, thus allowing the growth of sufficiently short-wavelength density perturbations according to the isobaric stability criterion (Balbus 1986). As found by Balbus & Soker (1989), nearly radial modes are also isobarically unstable. However, since the heating time scale is of the order of the flow time, the growth of the instability is algebraic rather than exponential, and the power-law index tends to be small. Thus, it is not clear how effective this instability would be.

Although damped Alfvén wave generation seems to be the most efficient *microphysical* mechanism for converting CR energy to heat, it may not provide enough thermal pressure to confine the filaments. The rate of conversion is regulated by the value of v_{CR}, which depends on the gas density and magnetic field strength. We will show below that very large values of the CR streaming speed, of the order of the wind velocity, are necessary to generate enough thermal pressure for cloud confinement at the required ionization parameter. However, we note that there are alternative "macroscopic" mechanisms for converting CR energy into thermal energy of the plasma, which are likely to operate in the wind but are very difficult to model in detail. For instance, if the background plasma initially has an inhomogeneous density distribution, e.g., because of nonstationary or nonuniform mass loading at the base of the wind, then neighboring regions with different densities will be accelerated at different rates by the injected cosmic rays. The flow will develop myriad (possibly weak) internal shocks, which will convert the fluctuations in kinetic energy density into heat. As a result of this process, the thermal pressure could approach equipartition with the CR pressure, although the bulk of the CR energy would still go into accelerating the mean flow.

2.3. *Constraints on the Mass-Loss Rate*

Mass is probably injected into the wind over a range of radii, and may come from a number of sources: evaporation or ablation from an accretion disk or dense clouds, mass released by collisions of clouds, mass loss by stars. Constraints on the mass-loss rate can be derived for two different scenarios. In the first it is assumed that the wind is driven through the sonic point by CR pressure, and in the second we consider a wind that starts out being thermally driven by X-ray heating, with CR pressure acceleration taking over at larger radii.

For the first scenario it is necessary that CR pressure becomes important in the subsonic regime. Inelastic *pp* collisions compete with adiabatic losses as the principal loss mechanism for cosmic rays in dense or slowly moving gas. In an accelerating flow the former dominate if the column density across an acceleration length scale (R_a) is too large:

$$n_p R_a > 2 \times 10^{24} v_9 \text{ cm}^{-2} . \tag{2.12}$$

Condition (2.12) places an upper limit on the column density of any region in a wind which can be accelerated effectively by trapped cosmic rays.

Losses due to *pp* collisions also limit the maximum CR pressure in a region of nearly static gas, which might provide a reservoir for the wind. By setting $H_{CR} \approx C_{CR}^{(pp)}$, we estimate

$$p_{CR} \sim \frac{L'_{CR}}{12\pi R^3 n_p c\sigma^{(pp)} K^{(pp)}} . \tag{2.13}$$

If p_{CR} is less than the thermal pressure p_{th}, then the total pressure $p_{CR} + p_{th}$ will generally decrease with decreasing density. In this case the flow may be in hydrostatic equilibrium or may be accelerated by thermal pressure, but the dynamical effects of CR pressure can be neglected. However, once the density decreases to the point at which p_{CR} exceeds p_{th}, it is clear from equation (2.13) that the density dependence of p_{CR} will lead to runaway expansion of the gas. This is one way in which nearly static gas can be injected into a CR–driven wind. Requiring that p_{CR} in equation (2.13) exceed p_{th} then gives the maximum possible thermal pressure for gas injected into the wind from rest by the action of CR pressure:

$$p_{th,max} \sim \left(\frac{L'_{CR} kT_i}{12\pi R^3 c\sigma^{(pp)} K^{(pp)}}\right)^{1/2} , \tag{2.14}$$

where T_i is the temperature of the injected gas. For each assumed value of T_i, we may place a lower bound on the ionization parameter ($\Xi \equiv L_\gamma/4\pi c R^2 p_{\rm th}$) in the injected gas,

$$\Xi_{\rm min} \sim 0.35\left(\frac{L_\gamma}{10L'_{\rm CR}}\right)^{1/2}\left(\frac{L_{46}}{R_{19}\,T_{i7}}\right)^{1/2}, \qquad (2.15)$$

where $T_{i7} \equiv T_i/10^7$ K. Recall that in order for cool gas at $\sim 10^4$ K to exist in pressure equilibrium with the wind, $\Xi_{\rm min}$ must be smaller than about 10–30 (depending on the shape of the extreme ultraviolet [EUV] spectrum and the strength of absorption edges). This condition is easily satisfied for mass injection at $R \gtrsim 1$ pc, provided that the bulk of the matter is injected "warm," i.e., with $T_i \gg 10^4$ K. The hotter the mass injection, the greater the maximum thermal pressure attainable in the flow and the better the chance for cool filaments to survive. A good candidate for preheating the injected matter is Compton heating by the central continuum, which can bring the material to a temperature close to the inverse Compton temperature ($\sim$a few times 10^7 K for typical AGN spectra). Alternatively, the injected gas could be heated to $T \gg 10^7$ K in some violent process such as a collision between stars or clouds. If mass injection occurred mainly at $R \gg 10^{19}$ cm, the mass source could be photoionized clouds or irradiated stellar photospheres.

Provided that the acceleration of the wind is not inhibited by gravity, the mass flux per unit area in the region where the Mach number is of order unity is given by $\dot{m} = \rho v \sim p/v_s$, where p is the total pressure and v_s is the velocity at the sonic point (Begelman, McKee, & Shields 1983). If the pressure is dominated by injected cosmic rays, we have $p v_s \sim H_{\rm CR}\, l/3$, where l, the path length along a streamline below the sonic point, is of the order of the sonic radius R_s for a flow which originates over a range of radii with $\Delta R \sim R$. Combining these two relations, we find that

$$\dot{m} \sim \frac{3p^2}{H_{\rm CR}\,R_s}\,. \qquad (2.16)$$

Since the pressure at the sonic point is less than the pressure at the base of the wind, which in turn is $\sim 2p_{\rm th,max}$ for the case we are considering, the mass flux per unit area at radii $\sim R_s$ is also limited,

$$\dot{m} \lesssim 9 \times 10^{-12} T_{i7}\, R_{s,18}^{-1}\ {\rm g\ cm^{-2}\ s^{-1}}\,, \qquad (2.17)$$

corresponding to a limit on the total mass flux through R_s of

$$\dot{M} \lesssim 1.8 T_{i7}\, R_{s,18}\ M_\odot\ {\rm yr}^{-1}\,. \qquad (2.18)$$

In the case in which CR energy does not drive the wind through the sonic point, but only "kicks in" to accelerate an already supersonic X-ray–heated wind from smaller radii, an upper limit on the wind mass-loss rate can be derived from the theory of Compton-heated winds (Begelman et al. 1983; Begelman 1985). Mass fluxes of the same order as equation (2.18), or larger, are readily obtainable on scales of order 1 pc or larger.

It is interesting to compare the limits on the mass-loss rate that are imposed by the mechanism that drives the wind with another limit that can be derived if the absorbing clouds are confined by the thermal pressure in the wind. The requirement that the ionization parameter in the wind has to be less than $\Xi_{\rm cool}$ leads to the condition that

$$\dot{M} > 1.5 v_9\, L_{46}\, T_9^{-1}\ M_\odot\ {\rm yr}^{-1}\,, \qquad (2.19)$$

where T_9 is the temperature of the wind in units of 10^9 K. The combination of this last expression with the previously derived limits seems to indicate that the mass-loss rate has to be close to the maximum possible value, and that thermal pressure confinement is possible only if the temperature of the wind is higher than 10^8 K.

We explore the structure of some simple wind models numerically in § 2.4. Here we briefly discuss some of the qualitative properties of such winds; further discussion may be found in Begelman et al. (1983) for the Compton-heated case, and in Eichler & Ko (1988) for "energized winds" in general. Such winds typically approach the sound speed close to the injection radius, and winds with constant mass flux pass the sonic point at low velocity and remain supersonic thereafter. Because of this, it does not matter for this part of the discussion whether the wind was Compton-heated or driven by CR pressure in the subsonic region. We may divide the supersonic region into two zones: the "strong heating" zone and the "weak heating" zone. In the strong heating zone the energy deposition more than offsets adiabatic losses, and the specific internal energy in the wind (dependent on the ratio $p_{\rm CR}/\rho$ in a wind driven by CR pressure) increases strongly with radius (e.g., as a power of R). In the weak heating regime, $p_{\rm CR}/\rho$ decreases with radius because the internal energy input cannot compensate for adabatic losses. We first analyze the strong heating case. From the energy equations (e.g., eqs. [2.23] and [2.24] below) we see that $p_{\rm CR} \sim H_{\rm CR} R/v$, and the velocity scales according to

$$v^2 \sim \frac{\mathscr{M}_{\rm CR}^2\, H_{\rm CR}\, R^3}{\dot{M}}\,, \qquad (2.20)$$

where $\mathscr{M}_{\rm CR}^2 = 3\rho v^2/4p_{\rm CR}$ is the square of the cosmic-ray Mach number. Equation (2.20) is valid whether or not $\dot{M}$ is independent of R. The numerical coefficient in equation (2.20) depends on the radial dependence of $H_{\rm CR}$ integrated over the flow, and may be as large as $O(10)$. From the definition of $\mathscr{M}_{\rm CR}$ and $\dot{M} \propto \rho v R^2$, we can write $p/\rho \propto H_{\rm CR} R^3 \dot{M}^{-1}$. Since the specific internal energy must increase steadily in the strong heating zone, the self-consistency condition for this zone is that $H_{\rm CR}$ not decline with R faster than $R^{-3}\dot{M}$. If $\dot{M}$ is independent of radius, this condition is satisfied for the predicted neutron injection function shown in Figure 1, at R less than the order of a few parsecs.

A strongly heated supersonic flow accelerates rapidly ($dv/dR \sim v/R$). $\mathscr{M}_{\rm CR}$ remains of order unity, and the behavior of v is found by setting $\mathscr{M}_{\rm CR}$ at the order of a few in equation (2.20). If the heating is weak and $\dot{M}$ is approximately constant, then the flow can coast with increasing $\mathscr{M}_{\rm CR}$ but with v approximately constant. However, if $H_{\rm CR} R^3/\dot{M}$ decreases with R and $\dot{M}$ increases as a power of R, then the flow must decelerate.

2.4. *Numerical Wind Models*

In this section we present some simple spherically symmetric models of neutron-driven winds with constant mass flux. Neglecting diffusion of cosmic rays, and assuming $v_{\rm CR} < v$ (so that CR streaming is unimportant compared with advection), the steady state equations for the spherically symmetric two-fluid wind [to $O(u/c)$] are (compare Weymann et al. 1982)

$$\rho v R^2 = \frac{\dot{M}}{4\pi}\,, \qquad (2.21)$$

where v is the bulk fluid speed, ρ is the density of the thermal plasma, and $\dot{M}$ is the mass flux in the wind, assumed here to be independent of R;

$$v \frac{dv}{dR} + \frac{1}{\rho} \frac{d}{dR} (p_{\rm th} + p_{\rm CR}) + \frac{GM_{\rm BH}}{R^2} - \frac{H_{\rm CR}}{c\rho} = 0 , \quad (2.22)$$

where $M_{\rm BH}$ is the mass of the central black hole;

$$3v \frac{dp_{\rm CR}}{dR} - 4v \frac{p_{\rm CR}}{\rho} \frac{d\rho}{dR} - H_{\rm CR}\left(1 - \frac{v}{c}\right) + C_{\rm CR}^{(\rm A)} + C_{\rm CR}^{(pp)} = 0 ; \quad (2.23)$$

and

$$\frac{3}{2} v \frac{dp_{\rm th}}{dR} - \frac{5}{2} v \frac{p_{\rm th}}{\rho} \frac{d\rho}{dR} - C_{\rm CR}^{(\rm A)} + C_{\rm th} = 0 , \quad (2.24)$$

where $C_{\rm th}$ is the net radiative cooling rate per unit volume of the thermal gas. We neglect the pressure of the Alfvén waves, which is likely to be much smaller than the pressure of the thermal plasma. For $H_{\rm CR}$, the rate of cosmic-ray energy deposition per unit volume, we use the expression

$$H(R) = H_0\left(\frac{R^4}{R_1 R_2} + \frac{R^3}{R_1} + R^2\right)^{-1} , \quad (2.25)$$

in which $R_1 = 3 \times 10^{18}$ cm and $R_2 = 3 \times 10^{19}$ cm. This function approximates the results from BRS shown in Figure 1 for a proton injection index $\Gamma_p = 2$. To the form of $C_{\rm th}$ given in equation (2.8), a term should be added representing atomic heating and cooling processes such as photoelectric heating and cooling by collisional excitation, which becomes important at low temperature. However, we will argue below that these processes are not likely to be important in determining the dynamical structure of the high-velocity part of the wind.

The conversion rate of cosmic-ray energy to thermal energy is not very well constrained (see § 2.1). We consider three cases in our numerical models: (1) No conversion occurs at all, which means that the cosmic rays lose energy only due to expansion: $C_{\rm CR}^{(\rm A)} = 0$. (2) Conversion is very efficient: $C_{\rm CR}^{(\rm A)} = H_{\rm CR}(1 - v/c)$. (3) An intermediate case in which $v_{\rm CR}$ is assumed to be a fixed fraction of v and $C_{\rm CR}^{(\rm A)}$ is given by equation (2.4).

Critical wind solutions, which start subsonically and become supersonic, can be calculated if one specifies the injection radius R_i, $\dot{M}$, $M_{\rm BH}$, $H_{\rm CR}(R)$, L_γ, and $T_{\rm IC}$, and in some models the CR streaming speed $v_{\rm CR}$. We integrated equations (2.21)–(2.24) outward from small radii, and determined the critical solution (going into the critical point) with a shooting method. We then extrapolated through the critical point and continued the integration outward. In the inner, high-density, and subsonic part of the wind some of the approximations used in equations (2.21)–(2.24) break down. The main problem is that as the density goes up atomic cooling becomes more important, and if mass flux conservation is enforced, the matter is likely to be thermally unstable and form a two-phase medium, consisting of cool clouds in a hot intercloud medium. In this case our thermal balance equation, which assumes a single temperature, is no longer adequate. To alleviate this problem, we simply neglect the atomic processes in the expression for $C_{\rm th}$, thus artificially forcing the medium to go to the Compton temperature at high densities. If the subsonic part of the wind is already dominated by CR pressure, and the clouds are effectively coupled to the hot phase by drag (§ 4), this will have no influence on the dynamics of the wind, since the density that enters the dynamical equation (2.22) can be taken to be the average density of the hot and cold phases. We will overestimate the thermal pressure, since the density in the Compton-heated phase in our model will be higher than if cloud condensations were properly accounted for. Since the point at which radiative losses become negligible compared with other terms in the thermal energy equation generally lies well inside the critical point, our neglect of atomic processes will not have a strong effect on the high-velocity part of the flow, where most of the broad absorption line profile is formed. Also, we have to keep in mind that distributed mass injection into the wind is quite likely at small radii, so that our assumption of constant $\dot{M}$ may not be correct near the base of the wind.

The models presented here assume the following parameters, unless otherwise noted: the injection radius is 0.1 pc, the wind mass-loss rate $\dot{M}$ is 10 $M_\odot$ yr^{-1}, the black hole mass $M_{\rm BH}$ is 10^8 $M_\odot$, the luminosity L_γ from the central source is 10^{46} ergs s^{-1}, $T_{\rm IC} = 3 \times 10^7$ K, and the neutron luminosity L_n is 6×10^{44} ergs s^{-1}. In models referring to case 3, $v_{\rm CR}$ must be taken to be as high as 50% of v to provide thermal pressure confinement for the BAL clouds (see eq. [2.11]); $v_{\rm CR}$ may be lower if other confinement mechanisms are important.

In Figures 2a, 2b, and 2c we display the hydrodynamical wind models that result from the standard parameters listed above and the three different types of coupling between nonthermal and thermal particles. Plotted are the velocity, the sound speed, and the temperature of the wind as functions of radius. The first conclusion we can draw from these pictures is that neutron injection is quite effective in driving a wind at large radii. The largest velocities are reached at scales of the order of 100 pc, i.e., well outside the region between 1 and 10 pc where most of the energy is injected. The terminal velocities in these models are not very high because we chose to use a rather high mass-loss rate and a conservative neutron luminosity. The acceleration process is quite efficient in the sense that most of the injected energy is converted into kinetic energy of the wind. In case 1, i.e., no conversion of CR energy into heat, this is to be expected, since the only way in which the relativistic particles can lose energy is by expansion, which means that the efficiency is 100% (apart from a small amount of gravitational potential energy). However, even in the case that all injected energy is converted directly to thermal energy, only 20% of L_n is lost due to Comptonization, and 80% ends up as kinetic energy of the wind. The neglect of atomic radiative losses will not affect this conclusion, since almost all energy is injected at radii where the density is so low that radiative losses are negligible. The high acceleration efficiency we find means that the terminal velocity of the wind will simply scale as $L_n^{1/2}\dot{M}^{-1/2}$.

We point out here that even if the thermal pressure is unimportant for the wind dynamics, it still has to be calculated because it is likely to determine the pressure and hence the ionization parameter in the BAL clouds. In Figure 3 we show the ionization parameter due to thermal wind pressure as a function of radius for the three dynamical models presented above. It is seen that only model 2, which has instantaneous conversion of CR energy to heat, can achieve ionization parameters that are comfortably below $\Xi_{\rm cool}$. As predicted by our analytic estimate, equation (2.11), case 3 with $v_{\rm CR}/v = 0.5$ gives marginally sufficient confinement. Note also that both model 2 and model 3 are quite successful in producing an almost constant ionization parameter over a wide range in velocity, which seems to be required by the observations (WTC; Junkkarinen, Burbidge, & Smith 1987). In § 4 we discuss other factors that might contribute to cloud confine-

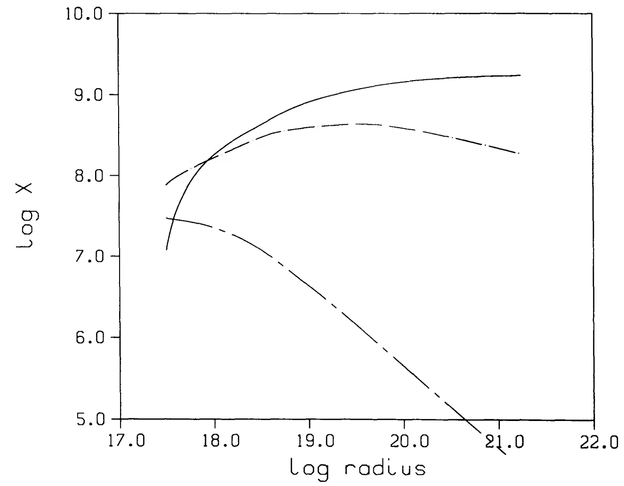

FIG. 2*a*

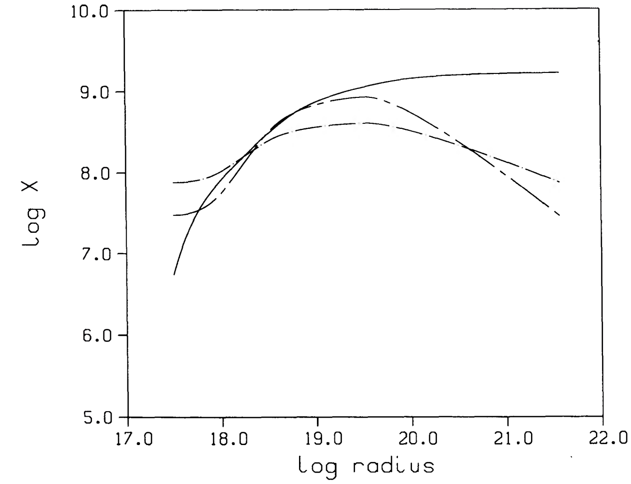

FIG. 2*b*

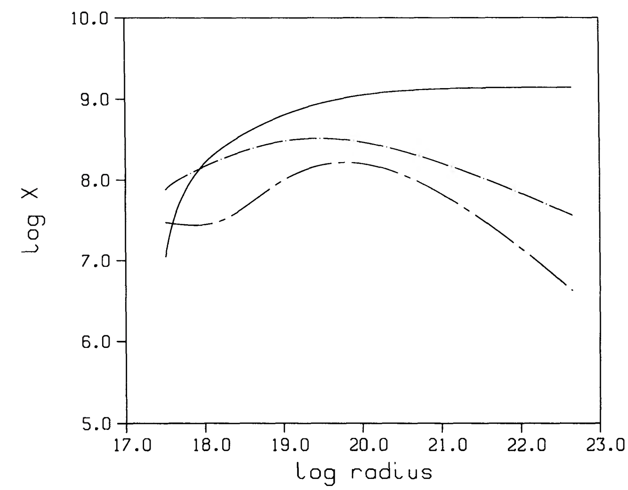

FIG. 2*c*

FIG. 2.—Some properties of the dynamical wind models. Plotted are the velocity (*solid curve*), the sound speed (*dot-dash curve*), and the temperature of the hot wind phase (*long-short–dashed curve*). All units are cgs. (*a*) Case in which no dissipation of cosmic ray energy takes place. (*b*) Instantaneous dissipation. (*c*) Dissipation given by eq. (2.4) with $v_{CR}/v = 0.5$.

ment, and show that CR pressure itself is almost certainly unable to confine such small clouds, even if the clouds are isolated magnetically from their surroundings.

3. BROAD ABSORPTION LINE PROFILES

In this section we will use the hydrodynamical wind models obtained in the previous section to calculate the BAL profiles that can be produced in these winds. As we have shown, the absorption must occur in relatively cool clouds that have a small filling factor. We calculate the line profiles under the following simplifying assumptions: the absorbing clouds move with the wind; the clouds have equal mass M_{cl}; the number flux of clouds as a function of radius $\dot{n}_{cl}$ is constant; the cloud temperature T_{cl} is $10^{4.5}$ K; the clouds are assumed to be in pressure equilibrium with the thermal pressure in the hot wind. As we saw in § 2.4, the conversion efficiency of CR energy to thermal energy has to be rather high in order to obtain a low enough ionization parameter. To obtain the line profiles shown in this section, we adopt the wind parameters from § 2.4, modeling the CR heating by case 2 because this yields ionization parameters that give the best agreement with observations.

If the clouds are roughly spherical, we can derive their size,

$$R_{cl}(R) = \left(\frac{3M_{cl}\,T_{cl}}{4\pi T_h \rho_h}\right)^{1/3} \tag{3.1}$$

(where T_h is the temperature of the hot wind phase) and their number density as a function of radius,

$$n_{cl}(R) = \frac{\dot{n}_{cl}}{4\pi R^2 v}\,, \tag{3.2}$$

which in turn determines the covering factor (i.e., the number of clouds in the line of sight between R and $R + dR$):

$$f_{cov}(R)dR = \pi R_{cl}^2\, n_{cl}\, dR\,. \tag{3.3}$$

The clouds are much smaller than the background source, and to calculate the line profiles we have to take both geometrical covering and covering in velocity space into account. We use the formalism developed by Kwan (1990) for this situation. The

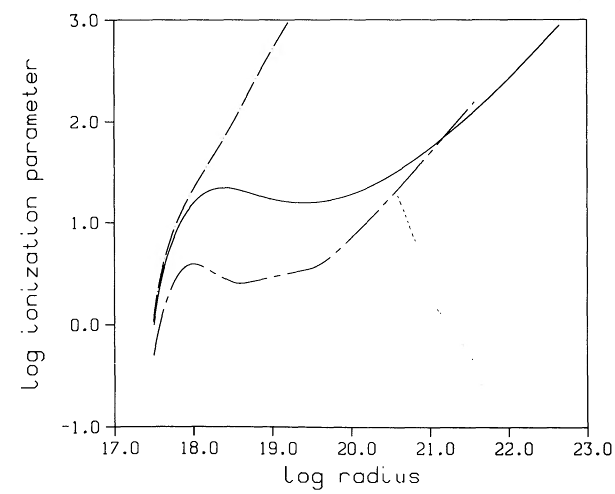

FIG. 3.—Ionization parameter as a function of radius for the three dynamical wind models described in the text. The dot-dash curve is for case 1, the long-short-dashed curve for case 2, and the solid curve for case 3.

intensity at the wavelength corresponding to a velocity shift v from the systemic velocity of the background source is given by

$$I(v) = I_0(v) \exp [-a(v)q(N_{\mathrm{cl},v}, b)] , \quad (3.4)$$

where $a(v)$ is the number of clouds in the line of sight per Doppler width at velocity v; $q(N_{\mathrm{cl},v}, b)$ is the average continuum depression ($\equiv [F_{\mathrm{cont}} - F_{\mathrm{line}}/F_{\mathrm{cont}}]$) over the line profile due to a single cloud with velocity v. It is given numerically by

$$q(N_{\mathrm{cl},v}, b)] \approx \tau_{c,v}(1 - 0.28\tau_{c,v}) , \qquad \tau_{c,v} < 1 ,$$
$$\approx [1.464 \ln(\tau_{c,v} + 0.43)]^{1/2} , \quad \tau_{c,v} \geq 1 , \quad (3.5)$$

where $\tau_{c,v}$ is the optical depth of the cloud at line center; $\tau_{c,v}$ is determined by the column density of the cloud in the ion that produces the line under consideration (N_{cl}) and the Doppler parameter b. Expression (3.5) is valid as long as the line is not strong enough to have damping wings. The derivation of equations (3.4) and (3.5) can be found in the reference cited above.

By using our previous dynamical models and specifying the mass-loss rate in clouds, $\dot{M}_{\mathrm{cl}}$, the mass of each cloud, M_{cl}, and the Doppler parameter b, we can calculate $a(v)$ and the hydrogen column density per cloud at velocity v. To obtain the BAL profile of a particular line, all that remains to be done is to determine the ionization equilibrium in the cloud at all velocities. To calculate this, it is assumed that the clouds are irradiated by a continuum from the central source which consists of the sum of an optical–to–soft X-ray power law ($F_\nu \propto \nu^{-1.4}$; Kriss 1988), an X-ray power law ($F_\nu \propto \nu^{-0.7}$), and a blackbody component with a temperature of 5×10^4 K. The power laws are assumed to be equal at 1 keV, and the thermal bump contains about as much power as the optical–to–soft X-ray power law. When calculating the ionization equilibrium as a function of radius, this spectrum is modified by absorption due to H I, He I, and He II in the interior part of the wind. Collisional ionization, by the CR particles as well as the hot thermal electrons (which may penetrate the clouds: see § 4.6), is found to be negligible.

If the clouds are assumed to be confined by the thermal pressure in the wind and irradiated by the unattenuated central continuum, the ionization level in the clouds is found to be somewhat higher than the optimum level for producing large amounts of species like C IV and Si V, except in the innermost, low-velocity part of the outflow. However, the high internal column densities observed in BALQSOs imply that absorption effects can modify this result. Since this column density arises mostly in the inner part of the flow, virtually all of the BAL–producing clouds are exposed to a significantly reduced ionizing continuum. Our results below confirm earlier suspicions (WTC) that the presence of a large absorbing column is conducive to the formation of broad absorption lines.

The exact shape of the continuum to which the clouds are exposed depends strongly on the degree of ionization of H and He (and hence the strength of the different absorption edges) in the absorbing column. The strong He II edge that we find in all of our models is very important, since this edge makes it very difficult to ionize C IV to C V, thus greatly enhancing the C IV column density. Because of the arbitrary nature of the inner radius of our wind model, and the thermal instability and mass loading effects discussed in the previous section that occur in the part of the flow where most of the absorbing gas is located, we cannot predict the shape of the ionizing continuum with certainty. In the models below these effects are parameterized by introducing a cutoff radius R_{cut}, inside of which $\dot{M}_{\mathrm{cl}}$ is assumed to increase linearly with radius from zero at R_{in} to the specified value at R_{cut}.

We take $\dot{M}_{\mathrm{cl}} = 10^{25}$ g s^{-1}, i.e., $\dot{M}_{\mathrm{cl}} = 0.015\dot{M}$, as a fiducial value for the mass-loss rate in cold material, and for the Doppler parameter b a value of 20 km s^{-1} is used. For this value of $\dot{M}_{\mathrm{cl}}$, the hydrogen column density of cool material in the entire outflow is of order 10^{22} cm^{-2}. This is in good agreement with the column densities derived for some BALQSOs from their soft X-ray absorption (Bregman 1984; Gioia et al. 1986; Singh et al. 1987).

The C IV and Si IV profiles presented assume that the local background continuum at the line position is the sum of a constant continuum and a broad emission line that consists of the two doublet components, with a peak flux equal to 1 and 0.5 times the continuum level and each having a width of 3000 km s^{-1}. We thus implicitly assume that the entire broad-line region is covered by the BAL region. We stress that because of the many uncertainties and simplifications (especially the assumptions of constant $\dot{M}_{\mathrm{cl}}$ and M_{cl}) our model cannot be expected to produce all the details of observed BAL profiles. Nevertheless, a variety of fairly realistic looking BAL profiles can be obtained.

When interpreting BAL profiles, it is useful to keep in mind that the column density at a certain velocity is proportional to the product of the hydrogen column density at this velocity and the ionization fraction. The hydrogen column density per unit velocity, which contains the effects of covering in velocity and geometrical space, is fixed by the dynamics. The ionization fraction depends mainly on the ionizing spectrum, on the internal absorption, and to some extent on the dynamics through the confining pressure. As we shall see from the profiles presented below, ionization effects can produce completely different line profiles for the same dynamical model, making it virtually impossible to constrain the dynamics from the observations.

The global behavior of the line profiles can be described as a function of two parameters, the amount of internal absorption and the mass of the individual clouds, with the boundaries between the different regimes depending on the other model parameters. For very low internal absorption the material tends to be slightly overionized, and it is difficult to produce very strong BALs, especially for Si IV. For very high internal absorption, on the other hand, the cloud material becomes underionized over a large range of radii, so that the BALs are strongest for intermediate ($N_{\mathrm{H}} \sim$ a few times 10^{21}–10^{22} cm^{-2}) absorption. The mass of the individual clouds, M_{cl}, determines the geometrical covering. As long as M_{cl} is less than a critical value (about 10^{17} g for model 2, with $\dot{M}_{\mathrm{cl}}$ equal to 10^{25} g s^{-1}), geometrical covering is complete at all velocities and the profile becomes independent of M_{cl}. For M_{cl} larger than this critical value, the profile starts to be modified by less than complete covering of the source, and the strength of the line is reduced. For dynamical model 2, the BALs virtually disappear for $M_{\mathrm{cl}} > 10^{20}$ g. Inside each regime sketched above, the BAL profiles are relatively simple, as illustrated in Figures 4, 5, and 6, which show C IV and Si IV profiles for the case of complete covering ($M_{\mathrm{cl}} = 10^{16}$ g) and increasing amounts of internal absorption (modeled by a decrease in the parameter R_{cut}).

In Figure 4 internal absorption is negligible, and, as mentioned above, our assumed spectrum makes the clouds too highly ionized to produce significant amounts of Si IV. In the case of intermediate internal absorption (Fig. 5) strong C IV and Si IV BALs are produced, although the C IV BAL is always

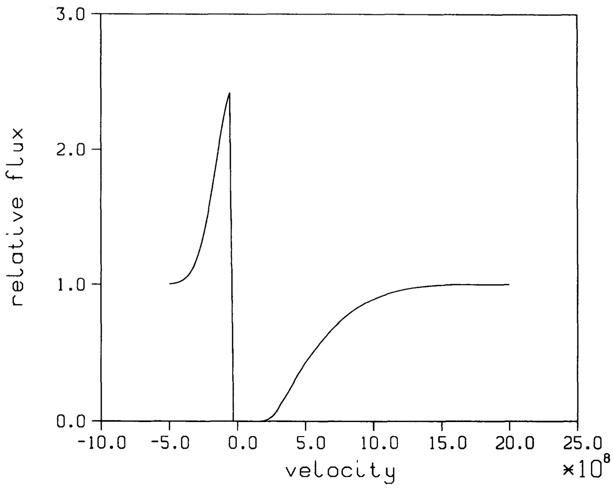

FIG. 4*a*

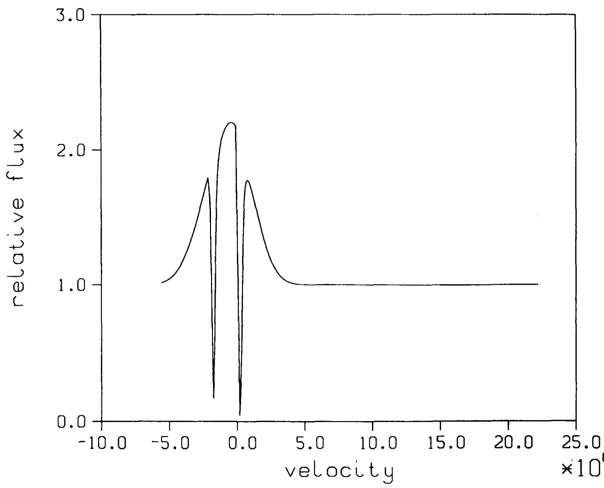

FIG. 4*b*

FIG. 4.—Calculated BAL profiles of (*a*) C IV and (*b*) Si IV based on dynamical model 2, for the case of negligible internal absorption, full geometrical covering at all velocities, and a mass-loss rate in cold material of 10^{25} g s^{-1}. Velocity standard is taken to be centroid of emission line; apparent negative velocities in absorption occur because lines are doublets.

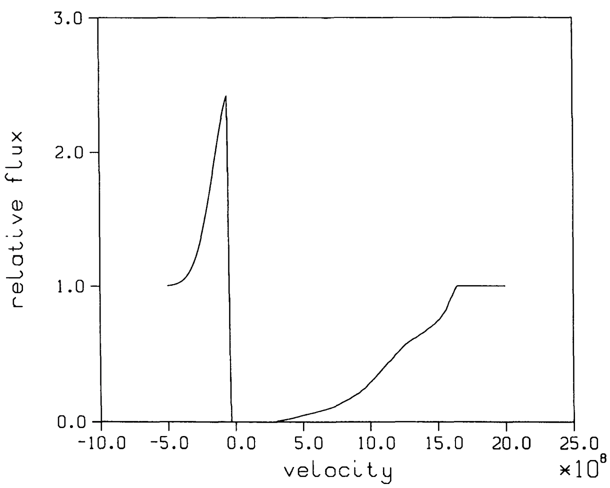

FIG. 5*a*

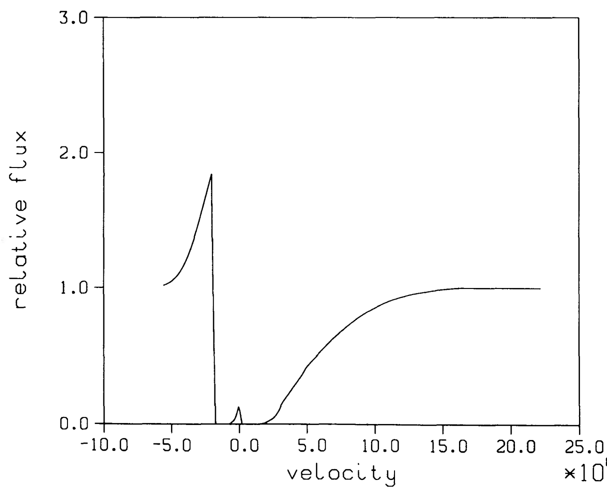

FIG. 5*b*

FIG. 5.—Same as Fig. 4, but with intermediate internal absorption

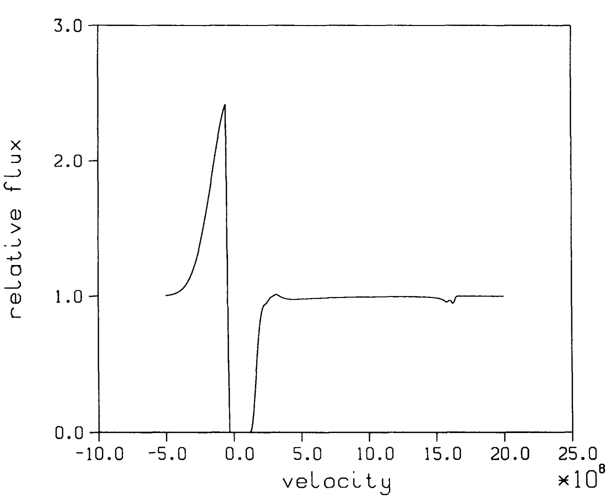

FIG. 6*a*

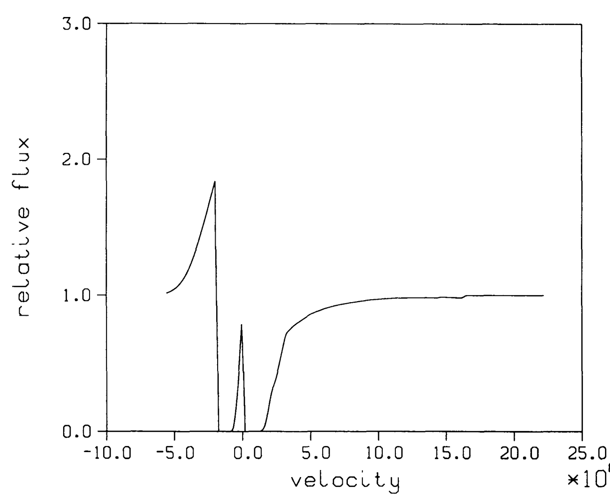

FIG. 6*b*

FIG. 6.—Same as Fig. 4, but with very high internal absorption

stronger than the Si IV BAL. The models represented by Figures 4 and 5 also produce fairly strong N V lines, with equivalent widths intermediate between those of C IV and Si IV. The problems associated with the simultaneous presence of strong Si IV and N V BALs is not completely resolved, however, because models that roughly reproduce the Si IV to N V line ratios always have much stronger C IV lines than observed. For very high internal absorption (Fig. 6) the clouds are underionized (apart from the small inner region that is not shielded from the central source), and the Si IV BALs can have a larger equivalent width than the C IV BAL. The small feature at high velocity in the C IV profile is caused by the increasing ionization parameter at very large radii. It is found for a range of parameters (compare Fig. 7), but it never becomes strong enough to provide an explanation for multicomponent BALs. Note that in many cases the large separation between the components of the Si IV doublet gives this line a larger equivalent width relative to C IV than would be expected from the column density ratio (Kwan 1990).

At the boundaries between the regimes more complex line profiles are obtained. In Figure 7 an effect occurring at the transition between medium and high internal absorption is illustrated. In this case rapid changes occur in the ionization equilibrium because of the fact that, as absorption edges grow stronger, some ionization coefficients change very rapidly whereas others are unaffected. Observationally, these jumps in the ionization equilibrium translate into steps in the absorption-line profile. Although obtaining very pronounced steps in the actual line profile requres some fine tuning, this example serves as a warning that line features like the steps observed in some BALQSOs with generally smooth line profiles, such as Q1413+113 (Turnshek et al. 1988), may not reflect dynamical or geometrical features.

In Figure 8 we illustrate what happens when the geometrical covering becomes incomplete. The profile is calculated for the same parameters as Figure 5, except that the cloud mass is increased to 10^{18} g. The source is now only partially covered at intermediate velocities, and the line profile is less deep. Note that effects like these are also able to produce profiles similar to those in Q1413+113.

Our theoretical BAL profiles have a number of properties in common with observed BALs, such as the fact that the absorption generally tapers off slowly to high velocity, in contrast to what is observed in stellar P Cygni profiles. In a few individual cases (mainly the PHL 5200 type BALQSOs) we can even obtain reasonable fits to the observations. Also, as should be expected of any model that roughly reproduces the observed BAL morphology, the cloud radii and densities that we predict are very similar to values derived observationally by WTC. However, there are many BALQSOs that have properties that cannot be reproduced by our model. One such property is a lack of absorption at low velocity. All of our models have a high optical depth at low velocities, because even a very low C IV or Si IV fraction cannot compensate for the geometrical effect that increases total column density at small radii. The simplest modification of our model that could give such behavior is to drop the assumption of constant M_{cl} and allow the clouds to be much more massive at low velocity, being ripped apart into smaller and smaller fragments as they are accelerated. In this case, the geometrical covering factor at low velocity could be small enough to suppress significant absorption. Alternative explanations could be found in a more complex geometry of the outflow, which almost certainly will not be spherically symmetric. Thus, it is possible that our line of sight to the central continuum source does not pass through the entire outflow, and selects only a certain range in velocities.

Another feature that cannot be explained by our model is the presence of multiple sharp absorption components. In the context of our model the most likely explanation for these components would be a variable or position-dependent $\dot{M}_{cl}$, but a deviation from spherical geometry as mentioned in the previous paragraph may also provide the explanation.

It has not been our purpose in this paper to provide detailed explanations of the observed BAL line ratios. The problems encountered in explaining these ratios are discussed in many publications (T88; WTC; Kwan 1990), and our relatively simple ionization calculations confirm most of them, such as the observed Lyα BALs being much weaker than predicted. Because our models already contain many parameters, we chose not to experiment with different ionizing spectra and concentrated on illustrating what kind of line profiles can be obtained. We would, however, like to make a comment here. In most studies (including this one), it has been assumed that the column density ratios have to be explained by material with a

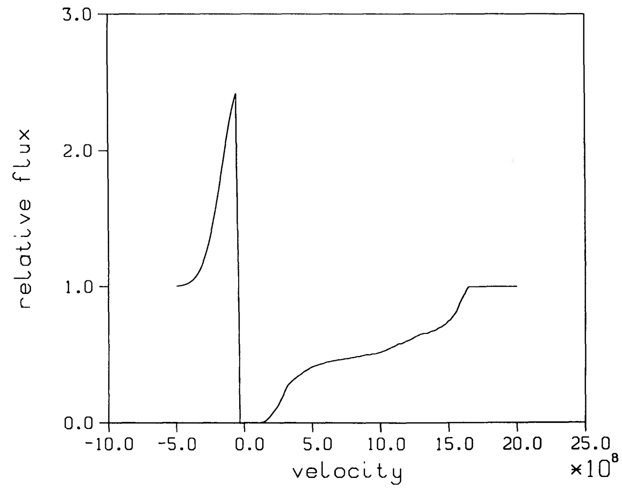

FIG. 8.—This C IV profile has the same parameters as Fig. 5, except that the mass is concentrated in larger clouds so that the geometrical covering becomes incomplete at intermediate velocities.

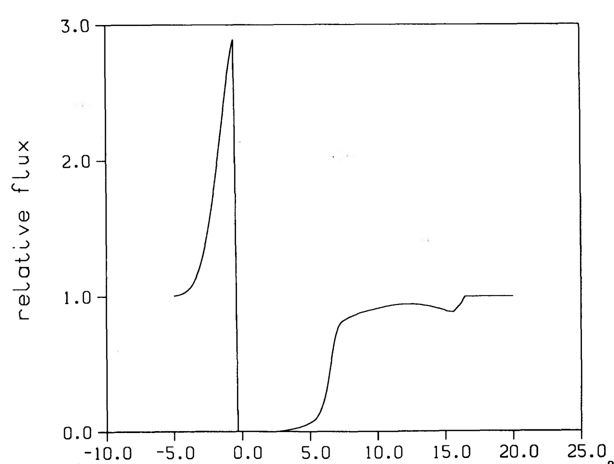

FIG. 7.—Example of a pronounced feature (in this case a sharp jump) in the BAL profile of C IV due to ionization effects.

unique ionization parameter at each velocity. In the simplest models this ionization parameter is taken to be constant throughout the BAL region, while in the more detailed ones the ionization parameter is taken to be a function of velocity. Even this latter approach may not have enough degrees of freedom for a realistic description of the BAL region, since we know that the absorbing clouds are much smaller than the background source. Thus, it is possible that the background source is covered by several regions with the same velocity but different ionization parameters, and the observed profile could be a composite of profiles from different lines of sight. Local variations in ionization parameter can be expected in our models if the confining thermal pressure is generated by shocks in the outflow. It should be investigated whether such a scenario can provide an alternative to abundance anomalies as an explanation for the observed line ratios.

4. CONFINEMENT, ACCELERATION, AND SURVIVAL OF ABSORBING GAS

4.1. *Overview*

Having shown that a simple model of absorbing clouds in a cosmic-ray–accelerated wind can explain many of the basic features of BAL profiles, we now address some of the theoretical problems and uncertainties connected with the presence of cool absorbing filaments or clouds in such winds. Many of the problems we face have been summarized elegantly in WTC. For reasons we enumerate below, we infer that the cool gas must be rather long-lived, in the sense that essentially the *same cool gas* must be accelerated with the wind from low velocities ($\lesssim$a few thousand km s^{-1}) up to the highest velocities observed. Because the cool filaments or clouds are too dense to be accelerated by the pressure gradient in the wind, they cannot be accelerated directly by CR pressure. Instead, they are presumably accelerated by a combination of the hydrodynamic ram pressure of the wind (possibly mediated through magnetic fields) and the pressure of the incident continuum radiation at the wavelengths of resonance lines. Since dense and possibly optically thick clouds accelerated by low-density gas and/or line radiation pressure are subject to Rayleigh-Taylor and Kelvin-Helmholtz instabilities, we must determine whether these filaments can survive despite the instabilities. We must also address questions of confinement and survival against thermal evaporation.

Some of the problems caused by instability would be alleviated if the clouds were continuously destroyed (e.g., by dynamical instabilities or evaporation) and new clouds reformed out of the hot phase by thermal instability. The newly formed clouds would comove with the hot phase, while most of the acceleration could occur while the protocloud material was part of the hot phase. However, there are at least two arguments against such a picture. First, at distances of $\sim$1 pc or more, the cooling time scales from high temperatures are longer than the flow time scales for any plausible mass flux. At distances very much less than 1 pc, the cooling time scales may be shorter than the flow time. However, in order to trigger thermal instability, the density would have to be so high that it would require an extremely large mass flux ($\gg$10–100 $M_\odot$ yr^{-1}). Models in which clouds are created by thermal instability behind shocks in the flow or around obstacles such as stars (Allen 1984; Perry & Dyson 1985) require cooling time scales which are much shorter than the flow time. We find these conditions implausible in view of the high velocities required in BALs, and we will not consider them further.

Alternative models requiring only short-lived clouds, but without the requirement of *in situ* cloud formation, have also been proposed (WTC). For example, cool gas could be entrained from approximate rest, e.g., from large clouds close to the line of sight, by a wind which is already moving at high speed. In this picture the breadth of the absorption troughs would result from the rapid acceleration of cool material in a few regions of width $\Delta R \ll R$. However, we see three problems with such a model. First, the mass flux requirements at fixed R are increased by a factor $\sim R/\Delta R$. Second, we would expect the BAL profiles to vary considerably on time scales of the order of a year or less; this is not observed. Third, the time spent by absorbing gas at low velocities is much shorter than the time spent at high velocities, which would lead to troughs which start out shallow close to the rest wavelength and deepen with increasing blueshift. Although this behavior is sometimes observed, it is not a general feature (T88).

We therefore suspect that much of the cool gas present in the wind is picked up at relatively low velocities by entrainment from the ambient medium. An attractive source of cool gas would be the line-emitting clouds in the broad emission line region, which may well have a disklike geometry or even form the surface of a disk. For a wind accelerated over a length scale of order R, the required lifetime of the cool matter is of order $R/v \sim 300 R_{19} v_9^{-1}$ yr. The small inferred sizes of the filaments (§ 1) make it a challenge to justify such long survival times. First, there must be some form of pressure confinement. As we saw in § 1, the gas responsible for producing the broad absorption troughs must have a thermal pressure at least of the order of a few percent of the pressure due to the EUV and soft X-ray radiation from the central source, in order to remain at a sufficiently low temperature and level of ionization. In terms of the local CR pressure, this implies that

$$p_{\rm th} \gtrsim 0.3 \frac{L_\gamma}{L'_{\rm CR}} \left(\frac{\Xi_{\rm cool}}{10}\right)^{-1} \left(\frac{v}{c}\right) p_{\rm CR} . \tag{4.1}$$

Thus, for $L_n \lesssim 0.1 L_\gamma$ the thermal pressure in the clouds must approach 20%–30% of the cosmic-ray pressure as the wind nears terminal velocity. Maintaining this pressure during the acceleration of the wind requires some external confinement of the clouds, since the free expansion time which we estimate from the inferred cloud size is only of order 10^4–10^6 s. In the wind models discussed in §§ 2 and 3, we assumed that the clouds were confined by thermal pressure resulting from CR energy dissipation. Below we discuss and evaluate other possible contributors to cloud confinement. We first argue that cosmic-ray pressure, the main agent responsible for accelerating the wind, is *unlikely* to contribute significantly to cloud confinement, because the clouds are too small. We next consider the conditions under which magnetic and thermal pressure may dominate cloud confinement. If the gas is heated by damped Alfvén waves, the two forms of confinement are linked, because the heating rate is proportional to the Alfvén speed in the hot gas. Significant thermal pressure may also develop if unsteadiness in the neutron flux or mass supply leads to efficient shock heating throughout the wind.

Third, we consider the joint role that hydrodynamic drag and radiation pressure may play in accelerating and confining the clouds. If the clouds are accelerated hydrodynamically, we estimate that the ram pressure associated with this acceleration is one to two orders of magnitude smaller than the pressure required for confinement. However, we show that acceleration due to the radiation pressure at resonance-line frequencies can exceed the acceleration of the wind. The velocities of the clouds are then determined by a balance between radiative acceleration and deceleration by hydrodynamic drag. The contributions to cloud confinement by these forces may then be larger than in the case of pure ram-pressure acceleration but still turn out to be too small in general to confine the clouds. The natural tendency of the clouds to spread sideways (to "pancake") can be counteracted if there is a strong enough radial magnetic field.

We finally examine the susceptibility of clouds to disruptive processes such as hydrodynamical instabilities and thermal evaporation, and suggest some effects which may allow the absorbing gas to survive.

4.2. *Inability of Cosmic Rays to Confine Clouds*

Despite its role in accelerating the wind, the pressure of the trapped cosmic rays probably does not contribute much to cloud confinement. Indeed, the Larmor radius R_L of a typical CR particle injected locally is likely to be larger than the size of a cloud,

$$\frac{R_L}{R_{cl}} > 5 \times 10^4 L_{46}^{1/2} N_{cl,17}^{-1} \left(\frac{c_s}{v_A}\right), \tag{4.2}$$

where c_s and v_A are sound speed and the Alfvén speed within the cloud, respectively; the CR energy is taken to be the typical energy of a decaying neutron at R (cf. § 2.1); $N_{cl,17}$ is the cloud column density in units of 10^{17} cm^{-2}; and the inequality comes from demanding $\Xi < \Xi_{cool}$. Thus cosmic rays can penetrate the cloud even if the latter forms a narrow filament along the magnetic field.

The only way for CR particles to transmit a confining force to a cloud is through inelastic collisions with the protons in the cloud. This would be true even if the cosmic rays were well trapped by magnetic irregularities on scales much smaller than the cloud, since the cosmic rays are deposited evenly per unit volume by neutron decay. CR particles experience a higher *pp* collision rate inside the clouds than in the intercloud medium, owing to the higher density. If the time required for a CR particle to traverse the cloud is t_{tr}, then the resultant contribution to the confining pressure will be

$$\frac{\delta p}{p_{CR}} \sim 6 \times 10^{-5} \frac{t_{tr}}{t_s} N_{cl,17}, \tag{4.3}$$

where t_s is the sound crossing time across a cloud (evaluated at the cloud temperature). Thus, to attain $p_{th} \sim 0.1 p_{CR}$ would require confinement of individual CR particles for a time much longer than the sound crossing time across the cloud. Equation (4.2) implies that t_{tr} is likely to be close to the light-travel time across the cloud, so the force exerted is negligible.

4.3. *Confinement by Magnetic Pressure*

Rees (1987) has suggested that magnetic fields might confine the broad emission line clouds in AGNs; could a similar mechanism operate in BAL winds? Consider first a naive model for the scaling of the magnetic field strength with radius. In a radial wind with an initially random field direction, the tangential component of the field is expected to dominate at large radii, scaling as $B_t \propto (Rv)^{-1}$. Thus, as the wind accelerated, the ionization parameter of the clouds would increase in proportion to v^2, a trend which might be reflected in differences in the absorption profiles of different species as a function of blueshift: lower ionization levels should be more dominant at lower velocities, and vice versa. However, if most of the acceleration occurred within a decade or so of the injection radius, then the *radial* component of the field, which scales as R^{-2}, could dominate. The ionization parameter would then increase in proportion to R^2. Since the acceleration in our models occurs over a fairly broad range of radii, we would expect a correspondingly large spread in ionization parameters in this case as well.

Thus, the naive model for the scaling of B suggests that magnetically confined clouds would have the correct ionization level only within a fairly narrow range of radii and/or velocities. Unless the magnetic field in the wind started out particularly strong, we would expect the field to be too weak to confine cool clouds over much of the observed velocity range, unless there is some process which continuously amplifies the field in the outflowing wind.

Field amplification would probably result from the relative motion Δv between the clouds and the wind. This process would saturate when the magnetic pressure, p_{mag}, grew to a value of the order of the ram pressure, since at this point the magnetic tension forces would become strong enough to reduce Δv. As we show below (§ 4.5), the ram pressure is unlikely to be large enough to confine the filaments, hence this amplification mechanism appears to be unable to maintain the magnetic field strength at a level sufficient for confinement. We note that if heating by Alfvén wave damping were principally responsible for maintaining the pressure, then the Alfvén speed would have to be of the order of the flow speed, and field amplification would have to be strong enough to keep the magnetic pressure at a significant fraction of the CR pressure.

4.4. *Confinement by Thermal Pressure*

The only mechanism considered so far that seems to be able to provide the required confinement of the clouds is thermal pressure of the wind, provided that conversion from CR energy to thermal energy is very efficient. The high value of the CR streaming speed required to make excitation of damped Alfvén waves efficient enough leads us to suspect that dissipation of kinetic energy in shocks is the more likely mechanism to achieve this conversion (cf. § 2.2). As noted above, Alfvén wave heating would require very strong magnetic field amplification. If either process led to the equipartition of thermal and CR energy, then the observationally inferred ionization parameter for the clouds would be obtained naturally.

4.5. *Acceleration of Clouds by Ram Pressure and Radiation Pressure*

In our models for BAL profiles, we have assumed that the clouds are comoving locally with the wind. Since the wind is accelerating at a rate $g = v(dv/dR)$, the clouds must also be accelerated at the same rate. Typical values of g for our computed wind models are of order 0.01–0.1 cm s^{-2} at 1–10 pc. The forces capable of accelerating and decelerating clouds are the hydrodynamic ram pressure $\rho_h \Delta v^2$, directed opposite to the relative velocity Δv between the cloud and the wind, and the radiation pressure of the incident continuum at the frequencies of resonance lines. The assumption that clouds are locked to the acceleration of the wind is valid provided that $\Delta v \ll v$. If this condition is satisfied and the clouds are accelerated primarily by ram pressure, then Δv is given by

$$\Delta v \sim (R_{\rm cl}\, g)^{1/2}\left(\frac{n_c}{n_h}\right)^{1/2} , \tag{4.4}$$

where n_c is the density of the cloud. For clouds accelerated by ram pressure, the ratio of ram pressure to thermal pressure is given by

$$\frac{p_{\rm ram}}{p_{\rm th}} \sim \frac{gR_{\rm cl}}{c_s^2} . \tag{4.5}$$

Equation (4.5) defines a unique cloud size for clumps confined by ram pressure, for which $p_{\rm ram}/p_{\rm th} \sim 1$. However, a straightforward numerical estimate shows that $p_{\rm ram}/p_{\rm th} \lesssim 10^{-2}$ for clouds of the size inferred to exist in BAL regions, with g given by our wind models and $c_s \gtrsim 10$ km s^{-1}.

When the effects of line radiation pressure are included, the picture of cloud acceleration changes considerably (see Weymann et al. 1982 for another discussion of the effects of radiation pressure). The radiative acceleration as a function of radius for clouds of different masses is shown in Figure 9, for the same luminosity and spectrum used in the wind models of § 2. At a given radius, the maximum acceleration occurs for clouds which are optically thin to the main lines. The acceleration of the wind for model 2 is also shown on this figure. Apparently the resonance-line acceleration of optically thick clouds can exceed the wind acceleration throughout a significant part of the wind acceleration zone, for clouds with masses smaller than a certain value. For these conditions the radiative force will try to accelerate the clouds to a velocity greater than that of the wind, and hydrodynamic drag will provide a decelerating force to keep the cloud velocity just slightly greater than that of the wind. For an optically thick cloud the entire line luminosity is scattered and the radiation pressure is given by $p_{\rm rad} = L_\nu \Delta\nu_{\rm line}/4\pi R^2 c$, where $L_\nu \Delta\nu_{\rm line}$ is the luminosity absorbed in the line. Its value depends on the Doppler parameter of the cloud and the flux in the far-UV portion of the continuum, where the spectral shape is highly uncertain; as a rough guess, we estimate $L_\nu \Delta\nu_{\rm line} \sim 10^{-4} L_\gamma$. Balancing the

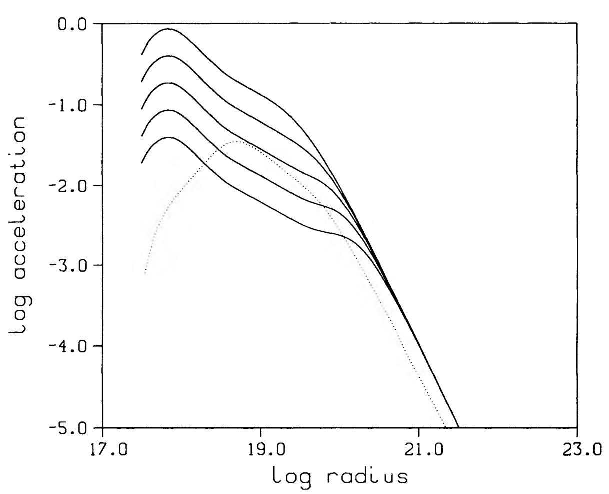

FIG. 9.—Acceleration of clouds by UV line radiation compared with the acceleration of the hot wind. The dotted curve represents the wind acceleration for dynamical model 2 as a function of radius, and the solid curves give the radiative acceleration of clouds with masses ranging from $M_{\rm cl} = 10^{14}$ g (*upper curve*) to $M_{\rm cl} = 10^{18}$ g (*lower curve*), with $\Delta \log M_{\rm cl} = 1$.

radiation pressure and the ram pressure, we find that Δv is given by

$$\Delta v \approx 6.9 \times 10^6 \times \left[\frac{(L_\nu \Delta\nu_{\rm line}/10^{42}\ {\rm ergs\ s^{-1}})v_9}{(\dot{M}/10\ M_\odot\ {\rm yr^{-1}})}\right]^{1/2} {\rm cm\ s^{-1}} . \tag{4.6}$$

This is clearly much smaller than the wind speed, justifying our assumption that the clouds are clearly comoving with the wind. Note that the role of the wind under these circumstances is to confine the clouds and to prevent them from being accelerated too rapidly, rather than to drag them along hydrodynamically. Independent acceleration of the wind is still necessary to prevent the drag forces from becoming too large.

Since both the drag force and the radiative force scale with the area of the cloud for an optically thick cloud, the "terminal velocity" Δv given by equation (4.6) is independent of cloud parameters. This means that even if a cloud fragments because of Rayleigh-Taylor instability, the fragments will not spread out in radius due to differential acceleration, provided that the fragments remain optically thick in the lines. However, since the drag and radiative forces act in opposite directions, they tend to squeeze the cloud between them. This squeezing force can exceed the force that would be obtained from ram pressure acceleration alone at a rate g, being of the order of the radiation pressure in the UV lines, but it is much smaller than the pressure required to confine the cloud. Another aspect of the squeezing force is that it is directed only radially, hence there will be a strong tendency for the clouds to spread sideways, or "pancake." This pancaking effect was discussed by Mathews (1982) in connection with the radiative acceleration of BEL clouds. If pancaking is not inhibited, a cloud should become optically thin in much less time than the radial acceleration time. The time scale for spreading is given by

$$t_{\rm sp} \gtrsim \left(\frac{L_\gamma}{L_\nu \Delta\nu_{\rm line}}\right)^{1/2} \Xi^{-1/2}\left(\frac{R_{\rm cl}}{c_s}\right) . \tag{4.7}$$

Once this happens, Δv will depend strongly on the column density of the cloud, and clouds can be disrupted rapidly by instabilities. Any mechanism which inhibits pancaking must exert more force on the sides of the cloud than on the front and back, therefore isotropic forms of pressure such as thermal pressure are not useful for this. Hydromagnetic forces could inhibit pancaking, provided that the field is predominantly radial and the magnetic pressure is of the same order as the ram pressure. As we argued in § 4.3, a radial field of this magnitude may be expected to develop as the result of dynamo effects.

For clouds with such high column densities that the radiative acceleration falls below the acceleration of the wind, there is no balance possible between radiative and drag forces. The clouds lag slightly behind the wind, with Δv being determined by the balance between the sum of drag plus radiation force (which now point in the same direction) and g. If hydrodynamical instabilities break the clouds into pieces, the differential drag forces will tend to separate the fragments, possibly leading to more rapid disruption of the clouds. However, if the fragments remain optically thick and become small enough that they move into the upper region of Figure 9, then their evolution may once again be stabilized by the balance between radiation pressure and drag.

4.6. *Survival against Hydrodynamical Instabilities and Thermal Evaporation*

As noted earlier, the small inferred sizes of the absorbing clouds make them particularly vulnerable to destruction by both hydrodynamical instabilities and thermal evaporation in the hot background plasma. The effects of magnetic fields alone are generally unable to suppress the linear development of Rayleigh-Taylor and Kelvin-Helmholtz instabilities for all wavevectors. The linear growth time for the Kelvin-Helmholtz or Rayleigh-Taylor instability is of order

$$t_{\rm KH} \sim \frac{R_{\rm cl}}{\Delta v}\left(\frac{n_c}{n_h}\right)^{1/2} , \tag{4.8}$$

which is much shorter than the acceleration time scale of the wind. The time scale for Δv to adjust to a changing cloud size or density, the "drag" time, is much longer than $t_{\rm KH}$:

$$t_{\rm dr} \sim \left(\frac{n_c}{n_h}\right)^{1/2} t_{\rm KH} . \tag{4.9}$$

Therefore, once a cloud begins to break up, its fragments tend to be subjected to a similar Δv. This, coupled with the fact that the instability time scale varies in proportion to the unstable wavelength, implies that hierarchical fragmentation to very small scales probably occurs within a few times $t_{\rm KH}$. At this point, thermal conduction should be able to mix the hot and cold phases microscopically. The seemingly fatal susceptibility of ram-pressure–accelerated clouds to Rayleigh-Taylor instability has been stressed by Allen (1984) and Weymann et al. (1982). However, we will argue that clouds may in fact be able to survive the instability under certain circumstances.

The nonlinear development of hydrodynamical instability will cause the envelope of the cool material that originally comprised the cloud to expand into the hot phase, i.e., the mean density of the cloud material decreases as it mixes with the background. However, this does not automatically mean that the cloud disappears as an entity. The characteristic random velocities induced by the instability are of order

$$\frac{R_{\rm cl}}{t_{\rm KH}} \sim c_s\left(\frac{p_{\rm ram}}{p_{\rm th}}\right)^{1/2} . \tag{4.10}$$

Since we argued that the ram pressure is generally much smaller than $p_{\rm th}$, this implies that the fragments of the cloud separate at a fraction of their internal sound speed. By the time most of the cloud material has mixed with the hot phase, its envelope will have expanded to at most a few times its original size. The density of the mixture will be, perhaps, one to two orders of magnitude lower than the original cloud density, and the corresponding temperature of the mixture (which has the same pressure as the original cloud) will be one to two orders of magnitude higher, i.e., of order 10^6 K or less. Thus, while the mixture is much warmer than the original cloud, it is far colder than the hot background medium. If the "mixed" cloud is able to cool down in less than the time required for further expansion, it may be compressed by the surrounding hot phase and thereby maintain its integrity as a cloud.

The cooling time scale of the "mixed" cloud depends sensitively on the mean density of the mixture, $n_{\rm mix}$. If the ionization parameter of the mixture is low enough to permit cooling at all, then the cooling function (for cosmic abundances) may be approximated by the expression $\Lambda \approx 1.6 \times 10^{-19}\beta T^{-1/2}$ ergs cm^3 s^{-1} (Raymond, Cox, & Smith 1976), where the parameter β represents effects due to deviations from coronal ionization equilibrium. Rapid mixing of hot and cold gas can lead to underionization, which can enhance the cooling significantly (McKee & Ostriker 1977), leading to $\beta \gg 1$, but the presence of a photoionizing radiation source will counteract the enhancement. The cooling time scale of the mixture is then given by

$$t_{\rm cool} \sim \frac{5}{2}\frac{kT_{\rm mix}}{n_{\rm mix}\Lambda} \sim 178\beta^{-1}\Xi T_{4.5}^{5/2} L_{46}^{-1} R_{19}^2 \left(\frac{n_{\rm mix}}{n_c}\right)^{-5/2} {\rm s} , \tag{4.11}$$

where T is the temperature of the cool gas before mixing and Ξ is its ionization parameter. By comparison, the instability time scale satisfies

$$t_{\rm KH} \lesssim 3 \times 10^6 \left(\frac{R_{\rm cl}}{10^{11}\ {\rm cm}}\right)^{1/2} \left(\frac{g}{10^{-2}\ {\rm cm\ s^{-2}}}\right)^{-1/2} {\rm s} . \tag{4.12}$$

Thus, values of $n_{\rm mix}$ as low as 0.01–0.1n_c may lead to cooling of the turbulent mixture rather than the complete dispersal of the cloud. We suggest that this may partially explain the longevity of clouds that appears to be necessary in models of BALs (Allen 1984; WTC).

Since the number of clouds along each line of sight is large ($\gtrsim 10^2$–10^4), even small relative velocities could lead to frequent collisions (time scale $t_{\rm coll}$) between clouds. Coalescence of clouds might be able to counteract fragmentation by hydrodynamical instabilities if $(t_{\rm coll}/t_{\rm KH}) \sim 1$. However, working out this ratio of time scales, we find

$$\frac{t_{\rm coll}}{t_{\rm KH}} \sim f_{\rm fill}^{-1}\left(\frac{n_h}{n_c}\right)^{1/2} , \tag{4.13}$$

which implies that coalescence would not be able to counteract fragmentation. Also, we estimate that the relative velocity Δv in the collisions is likely to be several times larger than the sound speed in the clouds, so that the collisions may lead to disruption rather than coalescence.

Even if clouds survive disruptive hydrodynamical processes, they are still subject to thermal evaporation. The evaporation rate depends on the ratio of the Coulomb mean free path of electrons in the background medium to the size of the cloud measured parallel to the magnetic field (Balbus & McKee 1982). Since the wind must be very hot in order to confine the clouds,

$$T_h \sim 3 \times 10^8 L_{46} v_9 \left(\frac{\dot{M}_h}{10\ M_\odot\ {\rm yr^{-1}}}\right)^{-1} \left(\frac{\Xi}{10}\right)^{-1} {\rm K} , \tag{4.14}$$

and the clouds are relatively small, this ratio is enormous. The "saturation parameter" of Cowie & McKee (1977), equal to roughly twice this ratio, is given by

$$\sigma_0' \sim 10^9 L_{46}^{-1} R_{19}^2 \left(\frac{R_{\rm cl}}{10^{11}\ {\rm cm}}\right)^{-1} \left(\frac{T_h}{10^9\ {\rm K}}\right)^3 \left(\frac{\Xi}{10}\right) . \tag{4.15}$$

If the clouds are magnetically connected to the surrounding medium, Balbus & McKee (1982) suggest that the hot electrons will diffuse into the interiors of the clouds. In this limit there is no "evaporation" in the normal sense, i.e., the deposition of heat in the surface layers of the cloud. Instead, Coulomb heating by hot electrons occurs throughout the cloud, at a rate given by

$$\Gamma_e \approx 3 \times 10^{-16} L_{46} R_{19}^{-2} \left(\frac{T_h}{10^9\ {\rm K}}\right)^{-3/2} \left(\frac{\Xi}{10}\right)^{-1} {\rm ergs\ s^{-1}} . \tag{4.16}$$

This heating rate can exceed the inverse Compton heating rate by more than two or three orders of magnitude. However, for the estimated cloud densities it is at least a factor of 10 smaller than the radiative cooling rate in the cold phase. If the ions are also able to penetrate the clouds, the heating rate could be as much as a factor ~ 20 larger, although penetration by ions is more likely to be inhibited by scattering off magnetic inhomogeneities.

5. SUMMARY AND DISCUSSION

We have shown how the escape of ultrarelativistic neutrons from the central engine of an AGN can lead to the production of a strong, fast wind with most of the acceleration occurring outside the broad emission line region. This feature is required in order to explain observations of BALQSOs, in which the blue wings of the BELs are often absorbed. A fine spray of absorbing cloudlets, accelerated along with the wind via a combination of hydrodynamical and radiative forces, yields BAL profiles similar to those which are observed. In order to maintain a sufficiently low level of ionization in the cloudlets to produce the absorption, it is necessary that a large fraction of the relativistic proton energy be converted to thermal or magnetic pressure, which confines the cloudlets. Photoelectric absorption of portions of the AGN continuum spectrum, possibly by gas in the inner parts of the wind, makes it easier to obtain the relatively low ionization levels observed.

The production of a powerful neutron flux, containing up to 10% or more of the bolometric luminosity of the AGN, is inevitable if the nonthermal acceleration of protons to ultrarelativistic energies is energetically important in the central engine. The electromagnetic output of a pair cascade triggered by relativistic proton injection is similar to that resulting from a pure electromagnetic cascade, which has been applied successfully to typical AGN continuum spectra by Zdziarski et al. (1990) (Stern, Sikora, & Svensson 1991). However, there is no strong evidence that proton acceleration is efficient in AGNs, nor is it known whether the injected proton energy distribution is sufficiently flat or extends to high enough energies ($\sim 10^5$ GeV or greater) for our model to be viable. Direct tests of the ultrarelativistic proton hypothesis would involve the detection of neutrinos with energies greater than 1 TeV (BRS) or very high energy gamma rays (Mastichiadis & Protheroe 1990), and will not be feasible for several years at least. Besides reflecting the primary injection function of protons, the energy distribution of escaping neutrons (and hence the radial distribution of energy injection in the wind) is shaped by the efficiency of neutron production (at low neutron energies) and the trapping of neutrons in the central engine by photomeson collisions (at high energies). These effects depend in turn on the detailed gasdynamics and radiative transfer within the central engine, which are not well understood. However, our conclusion (from BRS) that the energy deposition function should peak roughly in the range 1–10 pc should not be too sensitive to these details. Other factors, such as the decreasing gravitational force of the black hole and the decreasing importance of inverse Compton cooling with increasing radius, also favor a large radius for the wind acceleration zone.

For simplicity, we calculated spherically symmetric wind models. Although the neutron flux is likely to be nearly isotropic, the absence of detectable redshifted emission from the BAL clouds is strong evidence that the BAL region covers a solid angle of only ~ 1 sr. This also explains why the ultrabroad emission hump associated with the BAL material may be difficult to detect in the $\sim 90\%$ or more of radio-quiet QSOs for which our line of sight to the nucleus does not cross the absorbing material. Turnshek (1988) considers whether this partial covering is confined to a single region of the sphere, e.g., a cone or a disk, or consists of random patches. The fact that many cloudlets must lie along each line of sight within the BAL zone argues for a well-defined region, as does the presence of multiple troughs in many sources. In our model, the partial covering of the BAL zone presumably results from the angular distribution of sources of absorbing gas, which must be entrained by the wind. Outside the solid angle which contains the absorbing gas, we predict the existence of a fast (possibly relativistic), hot wind, but with a density so low that it may be virtually undetectable by direct observation. Since the wind carries such a large energy flux, however, it may be detectable through its interaction with the interstellar medium of the host galaxy or with the surrounding intergalactic medium, at distances well beyond the BAL region.

The inference that most radio-quiet QSOs possess BAL systems implies that the observed differences between BALQSOs and non–BALQSOs must be due to aspect effects. BALQSOs have been found to be more radio-quiet (Stocke et al. 1984), more highly optically variable over long (> 1 yr) time scales (Netzer & Sheffer 1983), and more highly polarized (Moore & Stockman 1984; T88) than their counterparts without BALs. The radio-quietness of BALQSOs may be partly explained in our model as being due to free-free absorption of the compact radio source by the absorbing cloudlets. The opitcal depths of the absorbing gas is given by

$$\tau_{\rm ff} \sim 10^2 T_{4.5}^{-5/2} L_{46} R_{19}^{-2} N_{\rm H,22} \left(\frac{\Xi}{10}\right)^{-1} \nu_9^{-2} , \qquad (5.1)$$

where $N_{\rm H,22}$ is the hydrogen column density in units of 10^{22} cm^{-2} and ν_9 is the frequency in units of 10^9 Hz. Since most of the absorbing column is located within 1 pc, we expect that the wind should become opaque at frequencies below 3×10^{10} Hz. However, if the structure and size of the compact radio source is similar to what is observed at better resolution in nearby AGNs, it is doubtful whether the strongly absorbing part of the wind will be able to cover the entire radio source. We have no explanation for why radio-loud QSOs (i.e., those with powerful extended radio sources) are not observed to have BAL systems. Since the extended emission from the radio lobes should be observable from any viewing angle, there must be *intrinsic* differences between radio-loud QSOs and BALQSOs.

We tentatively associate the other two observed features with the geometry of the BAL region. The relatively high level of polarization leads us to prefer a disklike geometry for the absorbing gas, since this would imply the BALQSOs are always observed at low inclination to the disk plane. If the BAL geometry were conelike, then it would be natural to infer that the viewing angle is nearly normal to the disk plane; hence the degree of polarization should be lower, not higher. A viewing angle close to the disk plane would also increase the probability that the central engine could be temporarily obscured by a large cloud, thus accounting for the enhanced level of slow optical variability.

Our model may not do justice to the full complexity of the BAL phenomenon, but we think it has some merit in trying to develop a global picture in which all steps leading to the formation of BALs have at least some physical basis. Further constraints on the origin of BALs will probably take a significantly larger amount of observational data than is presently available, especially variability information and correlations with properties in other wave bands.

This work was partially supported by NSF grant AST88-16140, NASA Astrophysical Theory Center grant NAGW-766, and the Alfred P. Sloan Foundation. M. C. B. and M. de K. thank the director of the N. Copernicus Astronomical Center in Warsaw, Poland, for extending hospitality and resources during a visit. M. S. thanks the Fellows of JILA for similar support.

REFERENCES

Allen, A. J. 1984, MNRAS, 210, 147
Balbus, S. A. 1986, ApJ, 303, L79
———. 1991, ApJ, 372, 25
Balbus, S. A., & McKee, C. F. 1982, ApJ, 252, 529
Balbus, S. A., & Soker, N. 1989, ApJ, 341, 611
Begelman, M. C. 1985, ApJ, 247, 492
Begelman, M. C., & McKee, C. F. 1990, ApJ, 358, 375
Begelman, M. C., McKee, C. F., & Shields, G. A. 1983, ApJ, 271, 70
Begelman, M. C., Rudak, B., & Sikora, M. 1990, ApJ, 362, 38 (BRS)
Blandford, R. D., & Eichler, D. 1987, Phys. Rept., 154, 1
Bregman, J. N. 1984, ApJ, 276, 423
Cowie, L. L., & McKee, C. F. 1977, ApJ, 211, 135
Eichler, D., & Ko, Y.-K. 1988, ApJ, 328, 179
Ferland, G. J. 1989, OSU Internal Rept. 89-001
Gioia, I. M., Maccacaro, T., Schild, R. E., Giommi, P., & Stocke, J. T. 1986, ApJ, 307, 497
Junkkarinen, V. T., Burbidge, E. M., & Smith, H. E. 1987, ApJ, 317, 460
Kirk, J., & Mastichiadis, A. 1989, A&A, 211, 75
Kriss, G. A. 1988, ApJ, 324, 809
Krolik, J. H., McKee, C. F., & Tarter, C. B. 1981, ApJ, 249, 422
Kwan, J. 1990, ApJ, 353, 123
Loewenstein, M. 1990, ApJ, 349, 471
Loewenstein, M., Zweibel, E. G., & Begelman, M. C. 1991, ApJ, 377, 392
Mastichiadis, A., & Protheroe, R. J. 1990, MNRAS, 246, 279
Mathews, W. G. 1982, ApJ, 252, 39
McKee, C. F., & Ostriker, J. P. 1977, ApJ, 218, 148
Moore, R. L., & Stockman, H. S. 1984, ApJ, 279, 465
Netzer, H., & Sheffer, Y. 1983, MNRAS, 203, 935
Perry, J. J., & Dyson, J. E. 1985, MNRAS, 213, 665
Raymond, J. C., Cox, D. P., & Smith, B. W. 1976, ApJ, 204, 290
Rees, M. J. 1987, MNRAS, 228, 47P
Sikora, M., Begelman, M. C., & Rudak, B. 1989, ApJ, 341, L33
Singh, K. P., Westergaard, N. J., & Schnopper, H. W. 1987, A&A, 172, L11
Skilling, J. 1975, MNRAS, 172, 557
Stern, B., Sikora, M., & Svensson, R. 1991, in preparation
Stocke, J. T., Foltz, C. B., Weymann, R. J., & Christiansen, W. A. 1984, ApJ, 280, 476
Turnshek, D. A. 1988, in Space Telescope Sci. Inst. Symposium 2, QSO Absorption Lines: Probing the Universe, ed. S. C. Blades, D. A. Turnshek, & C. A. Norman (Cambridge: Cambridge Univ. Press), 17 (T88)
Turnshek, D. A., Foltz, C. B., Grillmaier, C. J., & Weymann, R. J. 1988, ApJ, 325, 651
Wentzel, D. G. 1974, ARA&A, 12, 71
Weymann, R. J., Turnshek, D. A., & Christiansen, W. A. 1985, in Astrophysics of Active Galaxies and Quasi-stellar Objects, ed. J. Miller (Oxford: Oxford Univ. Press), 333 (WTC)
Weymann, R. J., Scott, J. S., Schiano, A. V., & Christiansen, W. A. 1982, ApJ, 262, 497
Zdziarski, A. A., Ghisellini, G., George, I. M., Svensson, R., Fabian, A. C., & Done, C. 1990, ApJ, 363, L1